Trace Element and Hf-Nd Isotope Constraints on the Origin of Young Tengchong Volcanic Rocks, SE Tibetan Plateau

by

Mingjia Ma

A thesis submitted to the Graduate Faculty of
Auburn University
in partial fulfillment of the
requirements for the Degree of
Master of Science

Auburn, Alabama
August 2, 2014

Approved by

Haibo Zou, Chair, Associate Professor of Geology and Geography
Willis E. Hames, Professor of Geology and Geography
Mark G. Steltenpohl, Professor of Geology and Geography

ABSTRACT

Hafnium and neodymium isotope systematics in mafic volcanic rocks provide useful information about mantle source characteristics and processes. Hf and Nd isotope arrays are useful for identifying the types of subducted sediments involved in enriched mantles. The Tengchong volcanic field is located in Yunnan Province and is one of two active volcanic fields on the Tibetan Plateau. Although a great deal of geochemical and petrological research has been conducted to investigate the origin of these volcanoes, application of combined Hf and Nd isotopes to study their mantle source characteristics has not been accomplished previously.

In this study, Hf and Nd isotopic compositions together with major and trace element concentrations are reported for the four active volcanoes in the Tengchong volcanic field, including Heikongshan, Dayingshan, Maanshan, and Laoguipo volcanoes. All studied samples have LREE enriched patterns. They are depleted in high field strength elements Ti, Nb, and Ta. Hf and Nd isotope results indicate that the Tengchong volcanics plot between the mantle igneous rock and seawater arrays. This implies that the enriched component in the mantle source for the Tengchong volcanic rocks was mature clay sediments or mudstones rather than other sediments such as sandstones. New constraints on the mantle source rocks from Hf-Nd isotope systematics in Tengchong can serve as a reference for interpreting the characteristics of the source rocks for older widespread post-collisional volcanism in other areas of the Tibetan Plateau.

ACKNOWLEDGMENTS

This research and field trip were supported by a National Natural Science Foundation grant of China (4127270) and a US National Science Foundation grant (EAR-1119077) to Haibo Zou. Thanks are owed to Qicheng Fan and Yongwei Zhao from Institute of Geology, China Earthquake Administration who helped me during my field work in Tengchong and laboratory studies in Beijing. Yueheng Yang is thanked for providing guidance and instruction on the operation of Hf liquid extraction and the multi-collector inductively coupled plasma mass spectrometry (MC-ICP-MS) at the Institute of Geology and Geophysics, Chinese Academy of Sciences. Thanks are also owed to Bei Xu from Peking University for grant reimbursement. I thank the Clean Lab at the University of Science and Technology of China for the measurement of whole-rock major and trace element concentrations. Special thanks go to my advisor Haibo Zou for providing the funding, materials, assistance in sample preparation, instruction on the extraction of Hf, and help in thesis writing. I also benefited from valuable suggestions and comments provided by thesis committee members Willis E. Hames and Mark G. Steltenpohl.

Thanks also go to my friends and colleagues at Auburn University. I also thank my boyfriend, Jingjing Zhao, for helping me with sample collection, data analysis, and for being extraordinarily supportive of my academic career. Finally, I am thankful to my parents for providing every kind of support throughout my studies and life.

TABLE OF CONTENTS

LIST OF TABLES

LIST OF FIGURES

INTRODUCTION

Explosive volcanic eruptions are catastrophic disasters to human beings, and the study of the origin and evolution of such magmatic systems has important significance to geology and society. The products of volcanic eruptions contain much information on magmatic processes, including source rocks, magma generation, evolution, migration and eruption processes. Detailed studies of volcanic rocks not only provide insights into the kinetics and dynamics of volcanic eruptions, but also play a critical role in the identification of source rocks, magma origin and evolution history.

The Tengchong volcanic field (TVF, 24°40′-25°30′N, 98°15′-98°45′E) is located in Yunnan Province of southwestern China, SE Tibetan Plateau, which is adjacent to Myanmar in the west and the Gaoligong Mountains in the east (Jiang et al., 2000; Zou, et al., 2010). It is one of the most intensively monitored active volcanoes in China and is one of two active volcanic fields on the Tibetan Plateau. This area is located above the leading edge of the subducting Indian plate, which has intense tectonic deformation, frequent magma intrusion activity, and a remarkable high-temperature geothermal anomaly. The Tengchong Cenozoic volcanic activity makes it significant for volcanology, geochemistry, and petrology. Maanshan, Dayingshan, Heikongshan, and Laoguipo are the four most recently active volcanoes in the TVF, each with recorded Holocene (<10 ka) eruptions. These volcanoes are considered dormant, but they still have eruptive potential.

Although a great deal of research has been carried out on many aspects of these

Tengchong volcanoes, application of combined Hf and Nd isotopes on whole-rocks samples is relatively lacking. Major and trace element and isotope studies of the magma can provide information regarding both the chemical characteristics of mantle sources and the tectonic history of extensional areas (Zou et al., 2000). Hafnium and neodymium isotope systematics in mafic volcanic rocks provide useful information about mantle source characteristics and processes. Hf and Nd isotope arrays are useful for identifying the types of subducted sediments involved in enriched mantles. During the evolution of the crust and mantle, Hf and Nd isotopic systems have different geochemical characteristics. Integrated research on the Hf and Nd isotopic system provides more comprehensive geochemical information of the crust and mantle evolution. Since young volcanic rocks such as those from the Tengchong volcanic field have only minor accumulations of radiogenic daughter isotopes after eruption, their isotopic composition can directly represent the isotopic characteristic of the source region without correction of parent isotopic decay (Zhou et al., 1998).

In this study, Hf and Nd isotopic compositions together with major and trace element concentrations are reported for the four active volcanoes in the Tengchong volcanic field, including Heikongshan, Dayingshan, Maanshan, and Laoguipo volcanoes. Results from the Hf-Nd isotope are compared with interpretations of mantle source characteristics based on ^{238}U-^{230}Th isotope disequilibrium data on the Tengchong volcanics (Zou et al., 2014). New constraints on the mantle source rocks from Hf-Nd isotope systematics in Tengchong have important implications for source rock

characteristics for older widespread post-collisional volcanoes in other parts of the Tibetan Plateau.

OBJECTIVES

This research focuses on the geochemical characteristics of volcanic rocks in the four youngest volcanoes of Tengchong, which are Maanshan, Dayingshan, Heikongshan, and Laoguipo. Field studies were performed to collect samples, whole-rock major and trace element analyses, and Hf-Nd isotope analyses were performed on these young lavas. The objectives of this research are three fold:

(1) To characterize composition of these young volcanic rocks to determine the volcanic rocks classification and the variation of the physical environment of the lava;

(2) To explore the enriched component in the mantle source for volcanic rocks, and to provide evidence of magma differentiation and crustal contamination;

(3) To place tighter constraints on the origin and evolution of the young Tengchong volcanic rocks.

BACKGROUND

Geologic Setting

The Tibetan Plateau primarily consists of the Kunlun, Songpan-Ganzi, Qiangtang, and Lhasa terranes from north to south, which were successively accreted to the Asian continent since Paleozoic (Fig. 1). Four principal volcanic age suites are identified: (1) Paleocene to Late-Eocene (65-40 Ma) volcanic rocks in the southern and central Tibetan Plateau; (2) Late-Eocene to Late-Oligocene (45-26 Ma) volcanic rocks in the central Tibetan Plateau; (3) Late-Oligocene to Late-Miocene (26-8 Ma) volcanic rocks in the southern Tibetan Plateau; (4) Late Miocene to now (8 Ma to the present) volcanic rocks in the northern and southeastern Tibetan Plateau (Xia et al., 2011). The Tengchong block is located between the Nujiang and Myitkyina suture zones along the southeastern margin of the Tibetan Plateau. The Tengchong block collided with Baoshan block during Yanshanian when the Meso-Tethys and Neo-Tethys Ocean had subducted. The Tengchong block is part of the southeastern margin of major tectonic deformation field of the Tibetan Plateau, which was formed by block rotation, escape, and strike slip faulting resulted from the collision between the Indian plate and Tengchong block during early Himalayan evolution. In the tectonic position, the Nujiang suture zone is the southern extension of the Bangong-Nujiang suture zone, and Myitkyina suture in the eastern Myanmar was connected with the Yarlung-Zangbo suture zone to the north, which was corresponded with Tengchong block and Lhasa block (Qi et al., 2011).

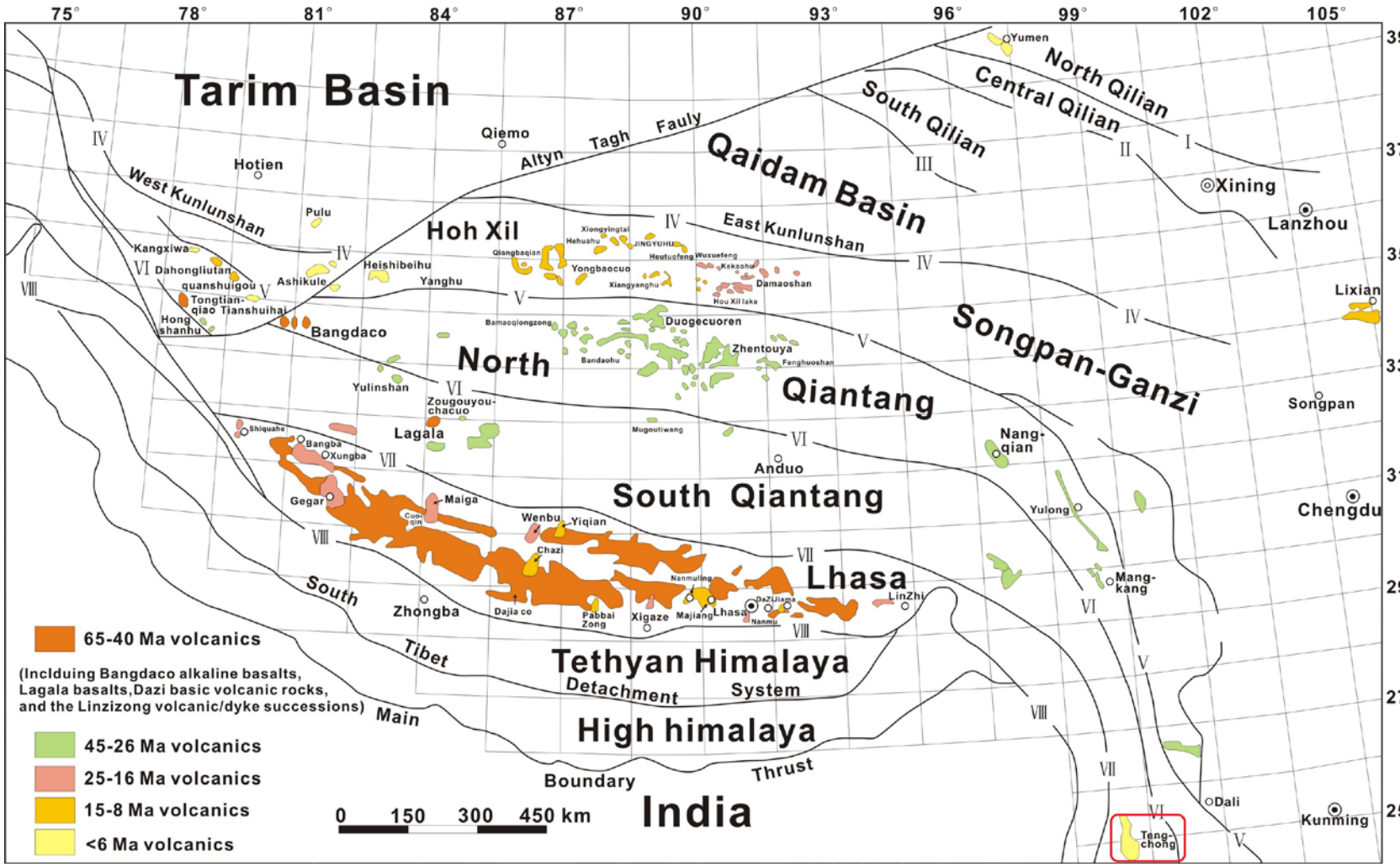

Figure 1. Simplified map of the Tibetan Plateau showing the distribution of Cenozoic volcanic rocks and the major terranes (after Xia et al., 2011). The Tengchong area is within the red box.

The Tengchong volcanic field is situated along the southeastern margin of the Tibetan Plateau near the border between China and Myanmar and adjacent to the Eastern tectonic area of the Himalayas (Fig. 2). It is one of the most famous young volcanic terrains in China, and the only volcanic geothermal area in the Himalayan geothermal belt. Tectonically, it is located on the Tengchong block to the west of the Nujiang River right-lateral strike-slip fault zone in the Three-Rivers area (Jiang et al., 2000). The lateral extrusion of the Indian Plate led to intense crustal deformation of the Tengchong block and adjacent regions.

Geotectonically, the Tengchong volcanic field is part of the Bomi-Tengchong fold belt of the Southern China pericontinental area. These two north-south continental interconnection belts from Bangong Lake to Nujiang River have experienced a complex collision and docking process during the late Paleozoic and Cenozoic (Wang, 1981).

The Tengchong volcanic field occurs in the northern part of the Tengchong-Lianghe area, spreading to the center of the Tengchong basin. The outcrop range of volcanic rocks is about 100 km from north to south, and 90 km from east to west. Rocks forming the crustal edifice into which the Tengchong magmatic rocks intruded are of multiple ages and types. The oldest units are Proterozoic Gaoligong Group metamorphic rocks, which are mainly dark green, gray-green sericite phyllite, schist, granite, and gneiss, outcropping sporadically and are greater than 1,000 m thick. The Carboniferous Menghong group consists of mudstone, slate, gravel greywacke, and dolomite, which are found only in the western Dayingjiang fracture, and are more than 3,000 m thick. Strata are missing after Carboniferous Menghong group deposition until Paleogene. The Paleogene Nanlin group represents continental clastics deposited unconformably above

the Yanshanian and Himalayan Granite and Proterozoic metamorphic rock. Mesozoic and Cenozoic magmatic activity is widely distributed and characterized by Yanshanian and Himalayan Granite, which are mainly classified as S-type, with minor I-type granites (Luo and Hu, 1983).

The Tengchong volcanic field comprises sixty-eight volcanoes of various sizes that are distributed in a South-North oriented strip of 50×90 km^2 (24°40′-25°30′N, 98°15′-98°45′E) (Jiang, 1998; Jiang et al., 2000). The four most recently active volcanoes in the Tengchong Volcanic Field (Fig. 3) are Maanshan (Fig. 4), Dayingshan (Fig. 5), Heikongshan (Fig. 6), and Laoguipo (Fig. 7), each with recorded Holocene (<10 ka) eruptions. These volcanoes are considered dormant, as they still have eruption potential. Volcanism in the Tengchong volcanic field has been divided into four different stages (Li, 1995; Jiang, 1998; Chen, 2003): (1) Middle–Late Pliocene olivine basalt (3.83 ± 0.72 m.y); (2) Early Pleistocene andesite and dacite (2.27–0.623 m.y); (3) Middle Pleistocene olivine basalt and basaltic-andesite (0.537–0.36 m.y); and (4) Holocene basaltic andesite and trachyandesite (Liu, 2000; Wei et al., 2003).

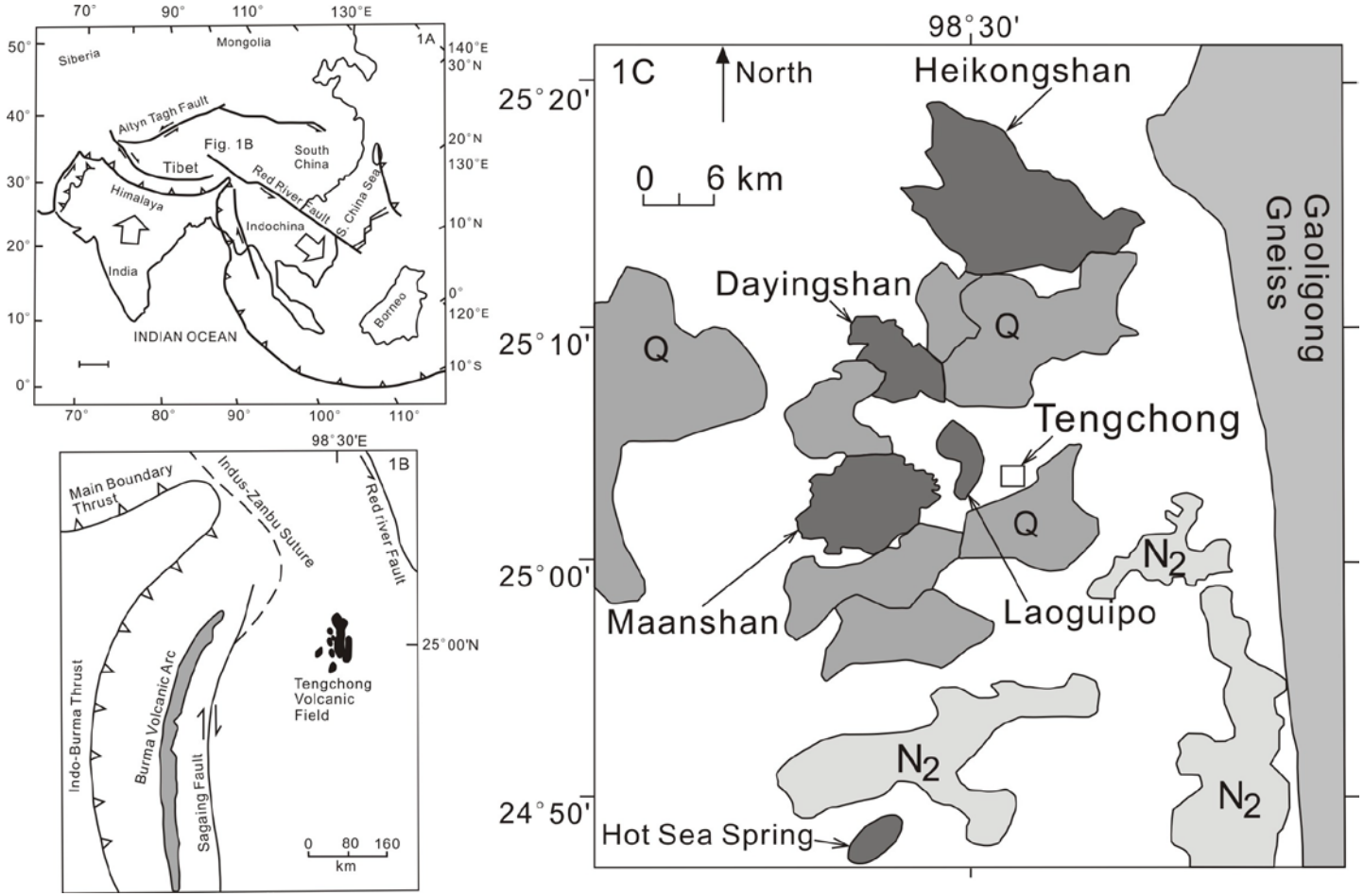

Figure 2. (a) Regional map showing major tectonic features in Asia (After Tapponnier et al., 1990). (b) Location map of the Tengchong volcanic field in SE China. TVF lies in an N-S trending fault zone between the Sagaing and Red River faults, and lies ~200 km from the subduction-related Burma volcanic arc. (c) Distribution and relative ages of the four most recently active volcanoes and surrounding rocks. Most volcanoes represented are small cinder cones (After Tucker et al., 2013).

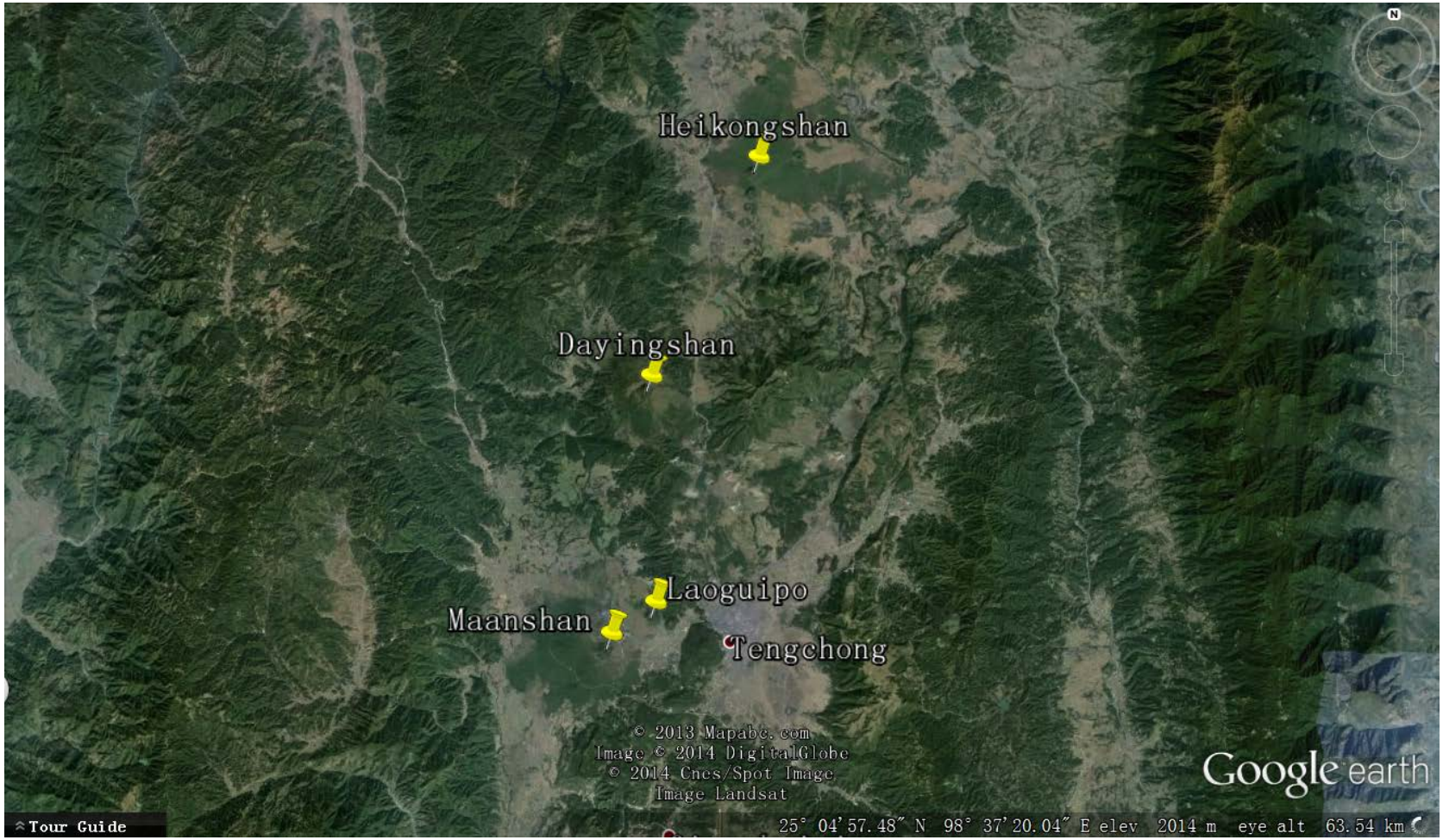

Figure 3. Distribution of the four Holocene volcanoes (Heikongshan, Dayingshan, Maanshan and Laoguipo) (From Google Earth).

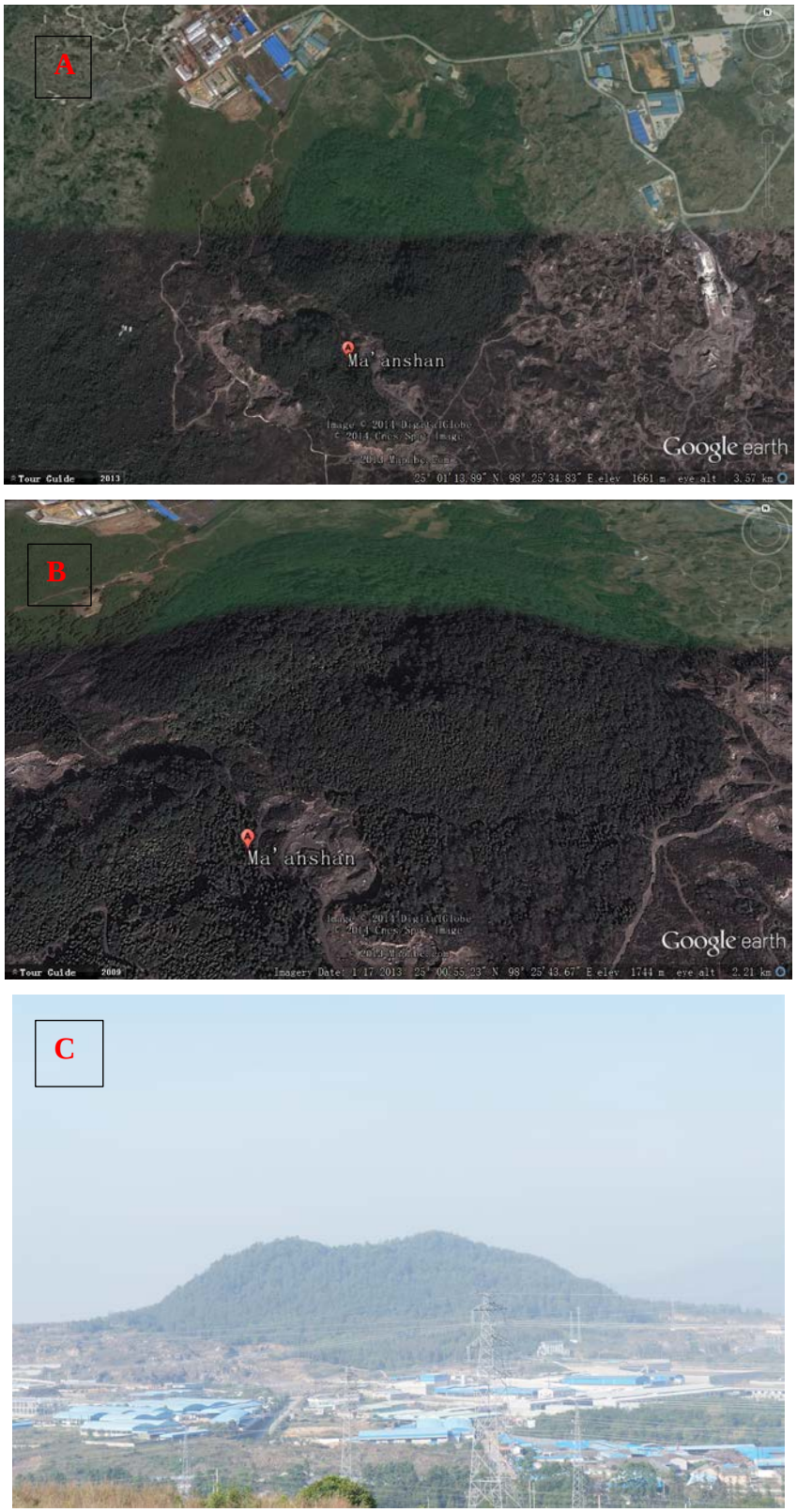

Figure 4. Maanshan volcano in the Tengchong Volcanic Field. A. Vertical view, north to top. B. Perspective view looking from south to north. C. Photograph illustrating shape of the cinder cone.

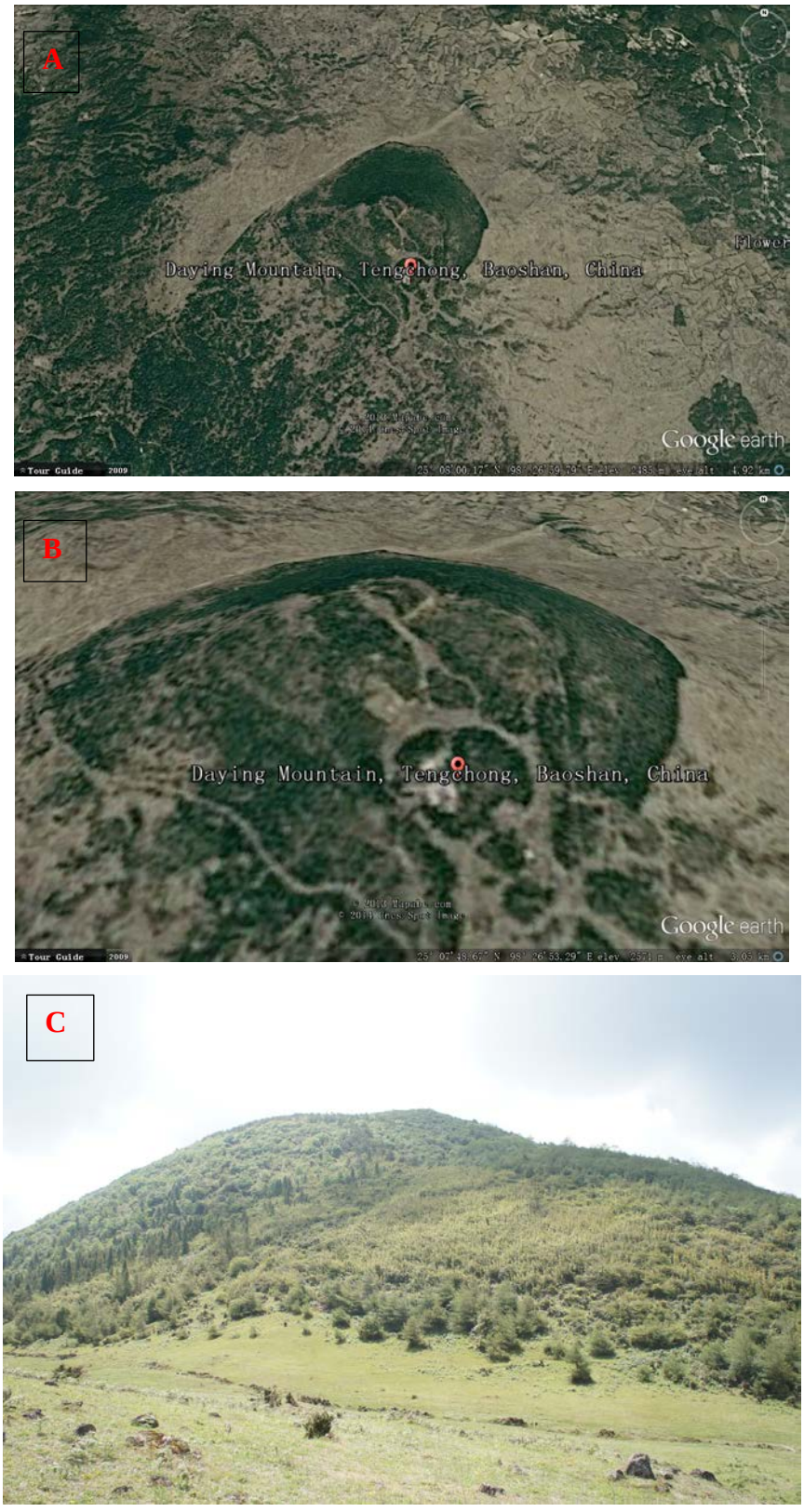

Figure 5. Dayingshan volcano in the Tengchong Volcanic Field. A. Vertical view, north to top. B. Perspective view looking from south to north. C. Photograph illustrating shape of the cinder cone.

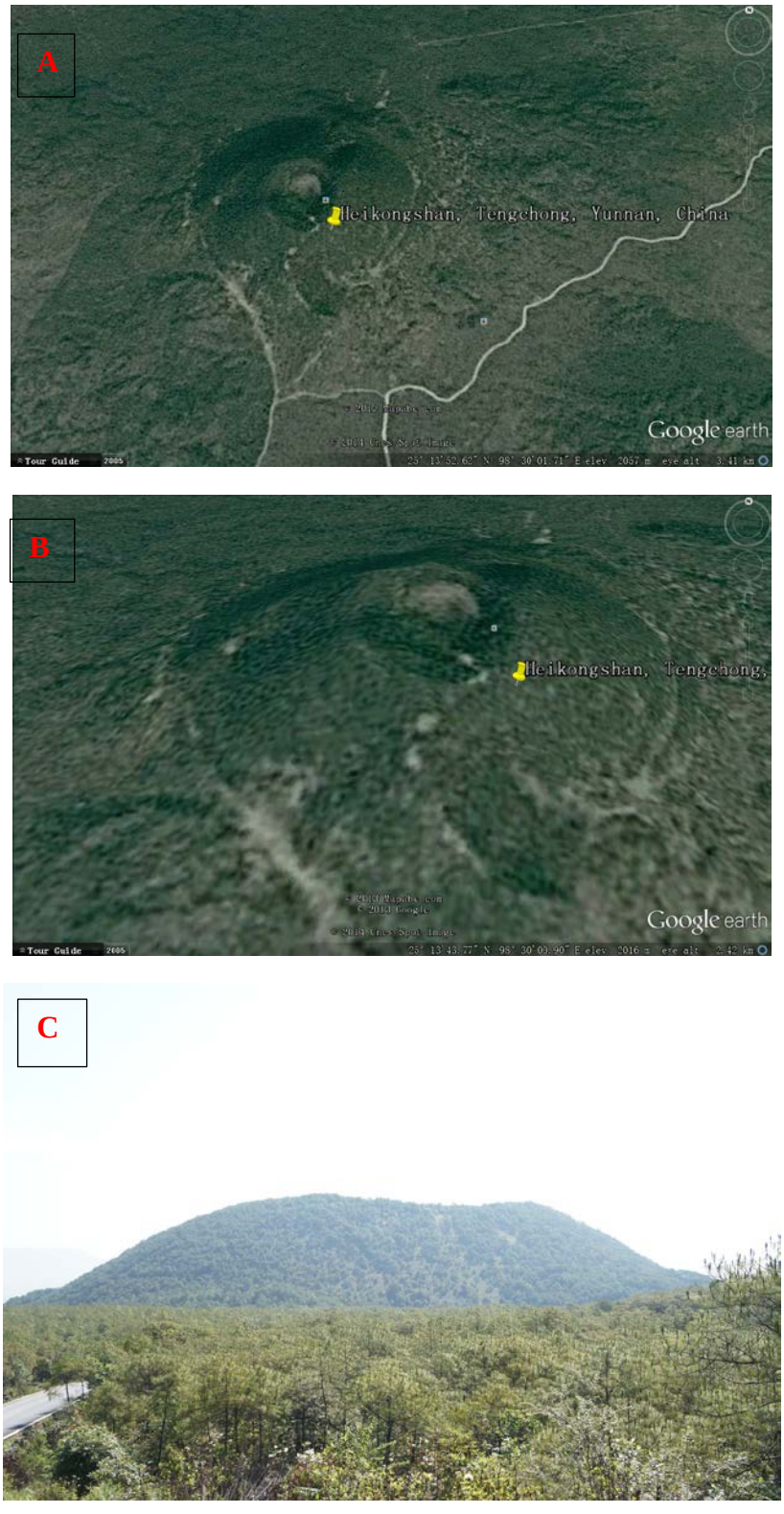

Figure 6. Heikongshan volcano in the Tengchong Volcanic Field. A. Vertical view, north to top. B. Perspective view looking from south to north. C. Photograph illustrating shape of the cinder cone.

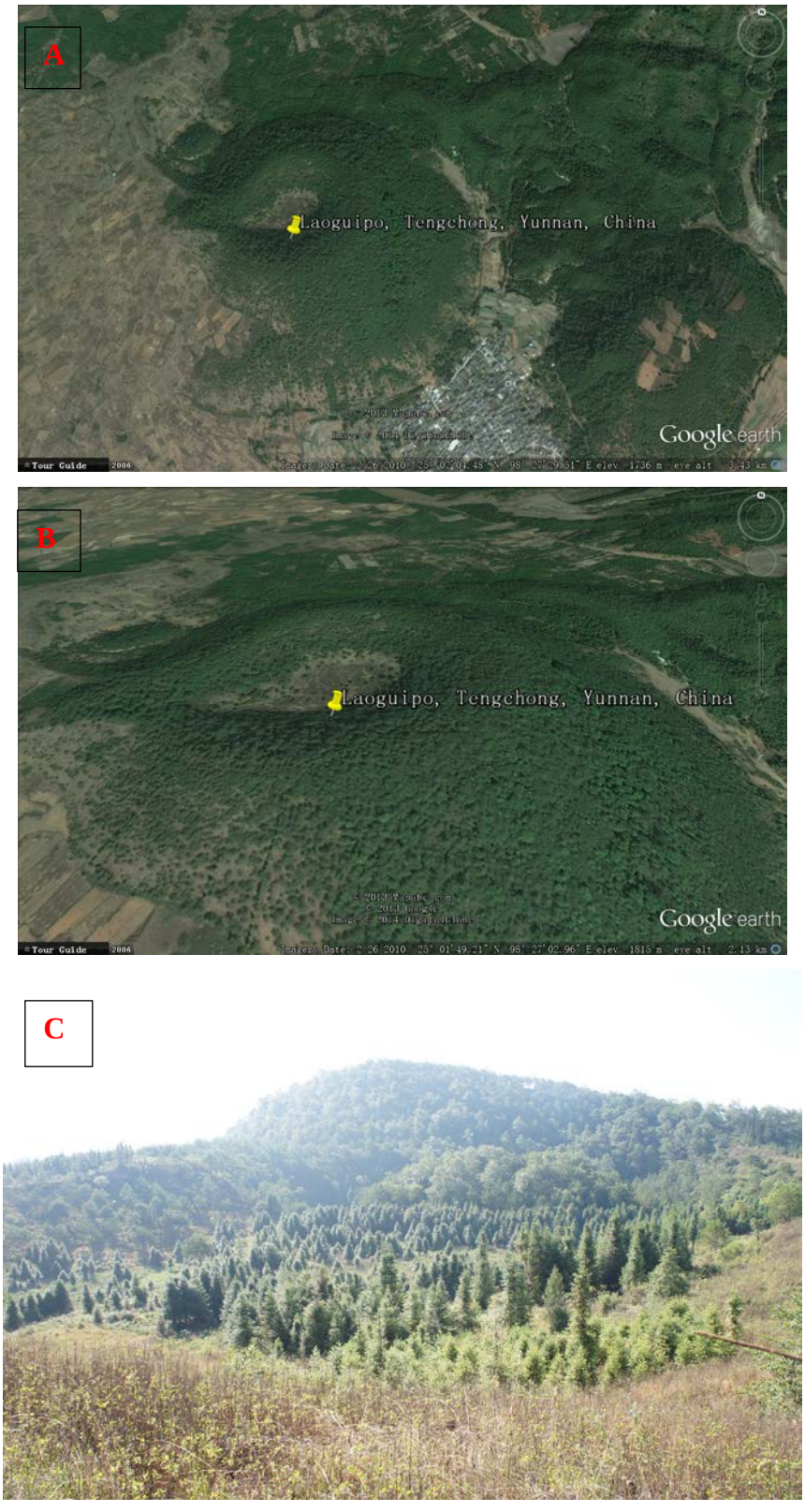

Figure 7. Laoguipo volcano in the Tengchong Volcanic Field. A. Vertical view, north to top. B. Perspective view looking from south to north. C. Photograph illustrating shape of the cinder cone.

Hf Isotope Principle

Lutetium (Lu) belongs to the Lanthanides group and is the heaviest of the rare earth elements. It has two natural isotopes: the stable isotope ^{175}Lu and the radioactive isotope ^{176}Lu, representing 97.41% and 2.59% of the natural Lu isotope abundance, respectively. Like all REEs, Lu is widely distributed and occurs primarily in phosphate, silicate, and oxide minerals. ^{176}Lu is unstable and decays by β-emission to stable ^{176}Hf, with a half-life of approximately 35 billion years. This phenomenon is the basis for the Lu-Hf method of dating and has also made Hf a useful isotopic tracer for the study of the origin of igneous rocks (Faure and Mensing, 2005).

Hafnium (Hf) is a High Field Strength Element (HFSE) and belongs to the Lithophile group IVB of the periodic table. It has six isotopes: ^{174}Hf, ^{176}Hf, ^{177}Hf, ^{178}Hf, ^{179}Hf and ^{180}Hf, all being stable non-radiogenic except for ^{176}Hf. The abundance of the isotope ^{176}Hf on Earth is variable due to the radioactive decay of ^{176}Lu, and in the literature it is conventionally compared to ^{177}Hf. The basic age equation for the Lu-Hf dating method, as applied to any closed system, is as follows:

$$(^{176}Hf/^{177}Hf)_t = (^{176}Hf/^{177}Hf)_{initial} + (^{176}Lu/^{177}Hf)_t * (e^{\lambda t} - 1)$$

where t is the elapsed time, and λ is the ^{176}Lu β-decay constant. Different values for λ have been proposed in the past by several authors. Patchett and Tatsumoto (1980b) proposed the value 1.94×10^{-11} y^{-1}, calculated from the slope of a Lu-Hf isochron for eucrite meteorites of known age. Sguigna et al. (1982) modified the λ value to 1.93×10^{-11} y^{-1}. Scherer et al. (2001) proposed a value of 1.86×10^{-11} y^{-1} obtained by calibration against the U-Pb decay system, which is in agreement with the value obtained by Nir-El

and Lavi (1998) using the decay scintillation counting method. The decay constant of ^{176}Lu is

$$\lambda = (1.94 \pm 0.07) \times 10^{-11}\ y^{-1}$$

The Lu-Hf isotope system is utilized to study the history of differentiation of the Bulk Silicate Earth (BSE) that led to the formation of the crust-mantle system. This isotope system has a systematic that is very similar to the Sm-Nd system, with some fundamental exceptions. The first is that, while Sm and Nd are both Rare Earth Elements with very similar chemical characteristics, Lu and Hf are respectively a Heavy Rare Earth Element (HREE) and a HFSE. This implies a very different behavior for Lu and Hf during the evolution of the crust-mantle system. Hf is more incompatible than Lu during the partial melting processes in the mantle; so, during the first events of juvenile crust generation in the Archean time, the crust has been enriched in Hf and depleted in Lu, leaving a mantle enriched in Lu and depleted in Hf. Thus, starting from an unique primordial mantle with chondritic Lu and Hf isotopic composition, which is referred as CHUR (Chondritic Uniform Reservoir) composition, two reservoirs with different Lu/Hf ratios were generated: the crust with $Lu/Hf_{crust} < Lu/Hf_{CHUR}$ and the depleted mantle with $Lu/Hf_{mantle} > Lu/Hf_{CHUR}$ (Massimo et al., 2010).

According to isotope tracer analysis theory, the similarity between Sm-Nd and Lu-Hf isotopic systems results in the positive correlation between Hf and Nd isotopes. The comparison of the $^{176}Hf/^{177}Hf$ ratio of a rock or mineral with the $^{176}Hf/^{177}Hf$ ratio of CHUR is expressed by the ε-value, defined as:

$$\varepsilon^0(Hf) = \left[\frac{\left(^{176}Hf/^{177}Hf\right)^0_{spl}}{\left(^{176}Hf/^{177}Hf\right)^0_{CHUR}} - 1\right] \times 10^4$$

Where

$$\left(\frac{^{176}Hf}{^{177}Hf}\right)^{0}_{CHUR} = 0.28286 \;\; at \; t = 0$$

Alternatively, the comparison can be made at some time *t* in the past. In that case

$$\varepsilon^{t}(Hf) = \left[\frac{\left(^{176}Hf/^{177}Hf\right)^{t}_{spl}}{\left(^{176}Hf/^{177}Hf\right)^{t}_{CHUR}} - 1\right] \times 10^{4}$$

Positive ε-values indicate that the sample is enriched in radiogenic ^{176}Hf compared to the chondritic reservoir and therefore originated from a source that had a higher time-integrated Lu/Hf ratio than chondrites. Similarly, negative ε-values are caused by a deficiency of ^{176}Hf and imply derivation from a source with a lower time-integrated Lu/Hf ratio than the chondritic reservoir (Faure and Mensing, 2005).

Hf Geochemical Characteristics

In all kinds of rocks, Lu is widely distributed and its abundance is rarely more than 0.5 ppm. The most important carrier minerals of this element are apatite, zircon, garnet, biotite, and monazite, while Lu abundance in the ordinary rock-forming minerals such as plagioclase, hornblende, pyroxene, and olivine is only at ppb levels magnitude. Among all types of igneous rocks, alkali-rich igneous rocks have particularly high Hf abundances, while the rest of the rocks have only 2-7 ppm Hf abundances. In a variety of minerals, Hf is considered as a dispersing element, replacing Zr (Ti in a few cases). Notably, the Hf concentration in zircon (0.5-2%) is much higher than other minerals. Low Lu/Hf values in common igneous rocks (0.2 or less) combines with limited current analytical precision (1%, 2σ) of ^{176}Lu/^{177}Hf, to make igneous rocks quite difficult to date using Lu-Hf, but it is feasible for garnet and apatite.

During partial melting of the mantle, Hf tends to be more concentrated in a siliceous melt than Lu, so the geochemical characteristics of Lu-Hf system is similar to the geochemical characteristics of Sm-Nd system. Thus, over geologic time, depleted mantle and crust show significant positive correlation variability between ε_{Hf} (t) and ε_{Nd} (t), which is called "Hf-Nd correlation" (Vervoort and Blichert-Toft, 1999). However, both Sm and Nd are REEs, such that the Lu-Hf system parent-daughter generally shows more significant differences in comparison to the Sm-Nd system parent-daughter during the mantle partial melting process. Moreover, due to the remarkably high Lu distribution coefficient of garnet (Johnson, 1998), long-term residual garnet in the melting process may destruct the "Hf-Nd correlation". However, the current observation of the lower crust granulite and garnet-peridotite mantle-derived rocks does not show "Hf-Nd correlation" decoupling (Vervoort et al., 2000). This suggests that garnet may not exist as the residual mineral in the melting process, and that the lower crust and garnet-peridotite mantle still have "Hf-Nd correlation" on the macro aspect. Otherwise, there is high Lu/Hf ratio and high $^{176}Hf/^{177}Hf$ ratio of garnet which does not get into the melt to be found by the researchers. According to the current research situation of crust and mantle, Lu-Hf and Sm-Nd systems are relevant (Vervoort and Blichert-Toft, 1999; Vervoort et al., 1999.).

In sediments, whether Lu-Hf and Sm-Nd isotopic systems are concordant is related to sedimentary environment. Based on the analysis of different ocean sediment types, Patchett et al. (1984) found that $^{147}Sm/^{144}Nd$ was constant 0.12-0.14, while $^{176}Lu/^{177}Hf$ in sandstone and clay display strong differentiation. Patchett et al. (1984) attributed this to the anti-differentiation of zircon with strong affinity to Hf to be

more concentrated in sand sediments compared to that in clay-rich sediments; REEs do not show such significant differentiation. Vervoort et al. (1999) found that the composition of Hf and Nd isotopes had obvious changes (nearly $35\varepsilon_{Hf}$ and $25\varepsilon_{Nd}$) between mudstone and sandstone in an active continental margin. The ε-value was mainly positive, but there was no differentiation between the two systems. $^{176}Lu/^{177}Hf$ values in sandstones and siltstones in passive continental margin were generally lower than the value of the mudstone, but both had similar $^{147}Sm/^{144}Nd$ values. These differences may result from zircon being stored in the passive margin sandstones (Stevenson and Patchett, 1990).

During metamorphism, especially under high-grade metamorphic or hydrothermal condition, the Sm-Nd system is often disturbed. On the other hand, the highly inactive character of Lu and Hf makes this system difficult to compromise for a metamorphic event following diagenesis, which makes it a reliable dating tool in high grade metamorphic rocks. Further, the initial Hf is more reliable than the initial Nd (Vervoort et al., 1996; Vervoort and Blichert-Toft, 1999).

PREVIOUS RESEARCH

Over the past 20 years Hf and Nd isotopic compositions have become an important tool to study volcanism source characteristics and deep mantle processes. Hf and Nd isotopes can provide a lot of information for source region partial melting and shallow magma fractional crystallization (Zhu et al., 2003). Hf-Nd systematics have been widely used and have contributed significantly in our understanding of many fields of geological investigation. Although much geochemical research has been carried out on Tengchong lavas, the previous studies mainly focused on Nd-Sr-Pb-U-Th isotopes. In recent years, the development of MC-ICP-MS technology allows for speedy measurement of Hf isotope concentrations, and the obtained information provides new insight into magma petrogenesis and other important geodynamic processes (Halliday et al., 1998; Blichert-Toft, 2001).

Hf Isotope Research

Hf isotope research began in the 1980s. Patchett and Tatsumoto (1980a) first established the proper method to separate and purify Lu-Hf from rock samples for thermal ionization mass spectrometry (TIMS) isotope analysis. These methods consume a sizable volume of the sample (Hf > 1 μg), and the internal precision of $^{176}Hf/^{177}Hf$ ratio analysis was not higher than 35 ppm, and $^{176}Lu/^{177}Hf$ ratio internal precision was 1-2%. Subsequently, Patchett and Tatsumoto (1980b) established a whole-siliceous earth initial $^{176}Hf/^{177}Hf$ ratio and a λ_{176Lu} decay constant through the establishment of the meteorite-sample Lu-Hf isochron method. They analyzed Lu-Hf isotope ratios of island arc basalts, old mafic rocks, and a large amount of zircon samples, and established a

global Hf isotope evolution line. During the process of comparing Lu-Hf to the similar Sm-Nd isotopic systems, Patchett et al. (1984) found that there was relatively high Lu/Hf in passive continental margin sediments. For several years, due to the low Hf ionization efficiency with TIMS (40,000 atoms ionized an atom), a great quantity of sample had to be consumed, the process involved complex separation and purification steps and a great deal of concentrated HF. Difficult instrumental analysis and measurement resulted in Lu-Hf isotope data coming mainly from zircon samples with low Lu and high Hf content, and only Patchett and a few other research groups reported success using the methods.

In 1990s, Salters (1994) established rock sample Lu-Hf separation and purification methods based on hot-secondary ion mass spectrometry (Hot-SIMS) isotope analysis, which provided internal precision of $^{176}Hf/^{177}Hf$ ratio analyses of 70-150 ppm levels for 50 ng Hf. Compared to the TIMs method, the Hot-SIMS ionization efficiency was improved nearly two orders of magnitude, greatly reducing sample consumption. However, Hot-SIMS instruments were only available in a very limited number of labs (essentially restricted to the Florida State University), and its chemical process was more complicated. Thus, this method was not widely used.

Blichert-Toft et al. (1997) first achieved rock samples Lu-Hf separation and purification methods based on MC-ICP-MS isotope analysis. Since MC-ICP-MS could effectively ionize Hf, the method allows a high analytical precision for samples as small as 10 ng Hf. As this report was written, many low Hf samples (including meteorites and peridotites) can be measured for Lu-Hf isotope using MC-ICP-MS. Blichert-Toft and Albarede (1997) used the meteorite Lu-Hf isochron method to redefine the whole-siliceous earth initial $^{176}Hf/^{177}Hf$ ratio and λ_{176Lu} decay constant. When combined with

Sm-Nd isotope data, they discovered that the whole-siliceous earth required a current undiscovered component to maintain its Hf-Nd isotopic mass balance (Blichert-Toft and Albarede, 1997). A host of researchers separate success using MC-ICP-MS and other separation and purification methods to analyze many terrestrial samples (Munker et al., 2001; Kleinhanus et al., 2002; Bizzarro et al., 2003; Ulfbeck et al., 2003; Li et al., 2005; Connelly et al., 2006; Massimo et al., 2010). All of these studies showed that the analysis of high Lu-bearing minerals such as apatite and garnet may allow for Lu- Hf isotopic age dating of host rocks. The LA-MC-ICP-MS technique provide rapid, micro-area, in-situ $^{176}Hf/^{177}Hf$ measurement in zircon because zircon Hf has the features of original Hf, when combined with U-Pb zircon SHRIMP Hf isotope analysis, it can record the source area and evolutionary history of host rocks of zircons (Knudsen et al., 2001).

Hf Chemical Separation

Lu-Hf isotope chemical separation technology was developed concomitant with advances made in Lu-Hf isotope mass spectrometry measurement technology. The technology for measuring Lu-Hf isotope in the early days was traditional TIMS, mainly focusing on geological samples with high Lu and Hf content, usually with acid-solubility methods. Patchett et al (1980a) applied the mixed acid to dissolve the sample through three sets of ion exchange separation of Lu-Hf. First, they used cation-exchange resin to separate the high-field-strength elements (HFSE) and rare-earth elements (REE), and collected the latter part of Lu component which contained few Yb atoms to measure Lu directly. Second, anion-exchange resin and different concentrations of HF acid were used to separate Zr, Hf, and Ti with a large number of matrix elements such as Cr, P, and Al. Third, H_2O_2, citric acid, and oxalic acid were used in complexing Zr, Hf, and Ti,

respectively, by cation-exchange resin in order to achieve complete separation of Zr, Hf, and Ti and the matrix element. Repeatedly recycled resin consumed high concentrations of HF acid (up to 25-29 N). Attention was placed before using the cation-exchange column in the third step because Hf is extremely easy to form complex anion with F- and it is not easy to be adsorbed by cation exchange resin. $HClO_4$ was required to thoroughly get out all the HF acid retained in the resin, otherwise it will seriously affect Hf recovery. The Lu recovery with Patchett's separating method was only 60% effective. Gruau et al. (1988) improved this method. He used α-hydroxy isobutyric acid leaching to allow complete separation of Lu and Yb by controlling the PH value of the solution, which improved Lu recovery. Salters (1991) used only concentrated HF to dissolve samples, and obtained Hf component through three sets of ion exchange column application. However, due to the repeated use of concentrated HF regeneration resin, the process blank was too high (500-1000 pg), which means the result is not satisfactory. Corfu (1992) improved on Patchett's method and developed chemical separation methods for zircon. Barovich (1995) established the Hf separation method based on Salters' studies, which was very suitable for high Ti (e.g. basalt) and high Zr (e.g. zircon) samples. That method used H_2SO_4 complex Hf, which reduced the loss of Hf using HF acid as complexing initially.

Salters (1994) used hot secondary ion mass spectrometry (Hot-SIMS) to measure Hf isotope composition. He applied concentrated HF acid to deal with samples when the samples passed through the ion exchange column and to make all Hf go into the solution phase. Salters (1994) then obtained the mixing components of Zr, Hf, and Ti by anion exchange column. Thus, in terms of the chemical separation methods in Hot-SIMS

analysis, the chemical separation process is highly demanding, and the ion exchange resin regeneration requires repeated use of concentrated HF acid as same as TIMS. After multi-collector inductively coupled plasma mass spectrometry (MC-ICP-MS) technology was developed in 1990s, it provides a solid basis for a variety of separation methods for the Lu-Hf isotope system.

The chemical separation and analytical techniques using MC-ICP-MS to measure Lu-Hf isotope system was developed by Blichert-Tolf (2001). It has very strict requirements for sample dissolution in Lu-Hf isotope (dating) measurement by MC-ICP-MS techniques. First, the key point of sample dissolution is to achieve complete isotope balance between the sample and the diluent. Due to differences in the behaviors of the elements, Lu is soluble in HCl but insoluble in HF acid, in contrast, Hf is soluble in HF acid but insoluble in HCl. Since it is added with Lu-Hf mixed diluent during the sample dissolution process, Lu and Hf can cause potential instability of the diluent due to the contradictory behavior of the elements in the same acid medium. Therefore, the preparation of Lu-Hf mixing diluent requires very careful processing. Another problem is that the sample must be thoroughly dissolved to achieve complete balance between the diluent and the sample. Moreover, because Lu and Hf in the rocks mainly occur in garnet, zircon, apatite, and other accessory minerals, the sample must be placed in the Teflon autoclave with metal covering to dissolve. The mixed acid of HF, HNO_3, and $HClO_4$ is used to dissolve the samples with caps open in 100-120℃ caps about 48 hours, concentrated HF is added to the dissolved and evaporated samples, and the beakers are placed on the electric hot plate overnight, which make the maximum Hf going into solution phase and make the rare earth element going into the solid fluoride. Fluoride is

separated by centrifugation, and then use HF acid to extract three times, which allows more than 90% of Hf going into the solution phase and part of the matrix elements and trace elements such as Ti, Zr, Nb, Mo, and Ta also into the solution phase. All rare earth elements and most of the major elements get into fluoride phase. This step enables the separation of REE and Hf, which reduces the interference of ^{176}Lu and ^{176}Yb in the mass spectrometry process. Then use ion exchange column twice to purify Hf. Use $HClO_4$ or HF, HNO_3, $HClO_4$ to re-dissolve the fluoride, apply HNO_3 and $H_2C_2O_4$ to purify Lu by cation exchange resin once, and finally employ it for MC-ICP-MS for mass spectrometry analysis (Wu et al., 2007).

Mixed acid dissolution method is difficult to guarantee complete Zr and Hf dissolution, especially for poorly soluble samples (such as garnet, zircon, etc.). However, the use of alkali dissolution method can not only effectively avoid those problems, but can also avoid the tedious steps for getting away all HF during the acid dissolution process. But the alkali dissolution method will bring more blank matrix and processes. Yang et al. (2000) used $LiBO_2$ alkali dissolution and resin separation method to note that both BHPA and Aliquat336 resins are able to effectively achieve the separation of Zr, Hf, and other matrix elements, but in terms of sample preparation and separation, BHPA resins are relatively simple and practical. Le Fevre et al. (2001) used $LiBO_2$ as the dissolvent, and applied U-TEVA resin to separate Ti and Zr and Hf effectively. Munker et al. (2001) used $LiBO_7$ to dissolve the sample, and then employed Eichrom Ln-Spec resin to separate Lu and Hf with passing the column once. Kleinhanns et al. (2002) used Na_2O_2 as the dissolvent to complete the separation of Lu-Hf and Sm-Nd once. Bizzarro et al. (2003) and Ulfbeck et al. (2003) also used $LiBO_2$ as the dissolvent to remove

matrix elements through $NH_3 \cdot H_2O$ precipitation, which can be further used for Sm and Nd isotopic analysis. Le Fevre et al. (2005) used $LiBO_2$ as the dissolvent to obtain the information of Sm, Nd, Lu, and Hf by four times exchange column, which avoided the cumbersome steps to deal with the samples several times.

Since 2000, Lu-Hf chemical separation methods continued to improve, and there was a one-time separation technique (Yona Nebel-Jcbsen et al., 2005). Meanwhile, scientists developed the chemical methods to separate Lu-Hf and Sm-Nd, U-Pb, and REE at the same time with different batches (Connelly et al., 2006), which meant one sample could provide much more information. According to the research needs, the chemical means of separating Lu-Hf, Sm-Nd, U-Pb, and REE from a single dissolution had been developed in order to provide sufficient information (Wu et al., 2007; Yang et al., 2010).

Hf Measurement Techniques

The application of Lu-Hf systematic to geosciences was developed since 1980 when Patchett and Tatsumoto (1980a) and Patchett et al. (1981) used TIMS to measure the respective isotopes. However, due to the high ionization potential of hafnium (6.65 eV), the TIMS method required large sample sizes and a high purity ion exchange separation in order to achieve acceptable results. In the last decade, the new MC-ICP-MS method, which permits excellent ionization on impure sample solutions, became the best method for Hf isotope analysis.

The earliest Lu-Hf isotopic studies were undertaken by conventional thermal ionization mass spectrometry of microgram quantities of purified Lu and Hf extracted from acid-digested samples via a series of cation-exchange columns (Patchett and Tatsumoto 1980c, Patchett et al. 1981, Corfu and Noble 1992, Barovich et al. 1995).

Despite hafnium's relatively poor ionization efficiency, the high Hf content of zircon makes TIMS analysis of multigrain zircon separates easy in comparison to most whole-rock samples. Precision of < 0.005% on the measured $^{176}Hf/^{177}Hf$ ratio was readily obtained from combined samples of tens to hundreds of grains. Fractionation was monitored by assessment of the invariant $^{179}Hf/^{177}Hf$ ratio measured on prepared standard solutions.

The first in situ micro-analytical technique developed for Lu-Hf isotope measurements was the SIMS method of Kinny et al. (1991), undertaken using the original SHRIMP (sensitive high-resolution ion microprobe) at the Australian National University. Hf isotopic abundances were measured sequentially on an electron multiplier as HfO+ species excavated from a 25-μm diameter area on individual sectioned zircon grains by a focused 10 kV oxygen ion beam. Counts taken on ^{176}Hf were corrected for the unresolvable spectral interferences ^{176}Yb and ^{176}Lu, and correction of Hf isotope ratios for instrumental mass fractionation was based on the measured $^{178}Hf/^{180}Hf$ ratio. As a result of the small analytical volume, the low ionization efficiency for Hf and the limitations of single-collector ion counting, the precision of the measured $^{176}Hf/^{177}Hf$ ratios was an order of magnitude poorer than TIMS analyses, typically 0.05 % (or ±5 ε-units), and consequently the method was not widely adopted. However, SIMS technology (VG ISOLAB) was utilized subsequently as a means of enhancing ion yields of bulk samples prepared in the usual manner for TIMS analysis, by bombarding samples loaded onto a heated Re filament with a 15 kV Ar ion beam (Salters, 1994).

Currently the most popular method for Hf isotope analyses is plasma source mass spectrometry (e.g., Halliday et al., 1995) in which the sample is presented to the ionizing

plasma either as an aspirated solution of chemically purified Lu and Hf (bulk method) or as material directly ejected from a zircon crystal by laser ablation (in situ method). In both methods, the sample aliquot is transferred to the mass analyzer (a double-focusing sector magnet) by a transporting gas, usually Ar. The combined isotope fractionation effects of the ablation/aspiration process and of the mass analyzer are monitored via internal and external standards.

The use of multiple Faraday Cup detector arrays in modern instruments compensates for plasma instability to the extent that internal precision now approaches that of routine TIMS analysis, with the added appeal of rapid analysis time. The popularity of ICP-MS has also led to development of improved chemical separation methods for Lu and Hf, optimized for the plasma source (Blichert-Toft et al., 1997) to the extent that single zircon grains containing as little as 25 ng of Hf can now be analyzed.

Research in Tengchong Volcanic Field

Since the 1980s numerous geologists have studied various aspects of the geochemistry, volcanology, petrology, and chronology of the Tengchong volcanic rocks. The majority of them focused on the enriched mantle by using the whole-rock major and trace elements, Nd, Sr, Pb, U, and Th isotopes (Zhu et al., 1983; Jiang, 1998; Fan et al., 2001; Zhou et al., 2000; Chen, 2003). Others made significant progress in constraining magma residence times using zircon U-Th disequilibrium age dating (Zou et al., 2010; Tucker, 2011; Yang, 2012). Crystal size distribution (CSD) and lava flow styles were also investigated as far back as thirty years ago. Whole-rock Hf-Nd studies, however, are relatively lacking.

Chen et al. (2002) analyzed Nd-Sr-Pb isotopic compositions of Cenozoic volcanic rocks from Tengchong to explore their petrogenesis. They also collected country rock samples that included amphibolites and Mesozoic to Cenozoic granitoids and measured their Nd-Sr-Pb isotopic compositions in order to evaluate the role of contamination and assimilation of country rocks during the formation of the volcanic rocks. They proposed that the origin of the Tengchong Cenozoic volcanic rocks is from partial melting of an enriched-mantle source, which probably resulted from assimilation of subducted slabs of the oceanic crust and sediments of the Neo-Tethyan basin. Crustal contamination during magma ascent apparently is not significant. Zou et al. (2010) suggested that the Tengchong volcanic magma was derived from enriched mantle formed by the subduction of continental crust, resulting in the negative ε_{Nd} (-7.0) and high $^{87}Sr/^{86}Sr$ (0.7076) in whole rocks from Maanshan. Zou et al. (2014) proposed that the Tengchong lavas with ultra-high Th/U ratios may come from a mantle source enriched by the clay-rich mature sediments from the modern Indian Ocean or the Neo-Tethyan or from the mudstones/shales of the subducted Indian continental plate.

Zou et al. (2003, 2007, 2010, and 2011) obtained zircon crystallization ages and magma residence time by both conventional in-situ U-Th dating of polished zircon grains and U-Th depth profiling of unpolished grains. They inferred that magma storage time was about 45 ka for the andesites from Maanshan, and zircon crystals shared common evolution instead of polybaric crystallization. Tucker's master thesis (2011), directed by H.B. Zou, focused on Dayingshan, and concluded that a magma chamber storage time of 48 ka is deduced by subtracting the most recent eruption age from the zircon age, because the Dayingshan zircons had two age populations at 58 ± 13 ka and 87.5 ± 6.5 ka. Yang

(2012) worked on the Heikongshan volcano, and recognized that the magma storage time was at least 57 ± 14 ka for the basaltic trachyandesite.

Yu et al. (2010) used crystal size distributions to recognize an undulating variation with the different units in Heikongshan volcano, which was intepretated to indicate multi-periods of magma replenishment. Their results also showed that trachyandesites from Heikongshan, Maanshan, and Dayingshan have totally different types of microstructures, bulk compositions, and contents of phenocrysts, which might suggest that they were from distinct magma chambers.

Zhao et al. (2012) identified three lava flow styles, including pipe flow, inflated flow, and laminar flow, in Dayingshang, Maanshan, and Heikongshan. Lava flows of the Dayingshan are characterized by pipe flow. Heat loss gradually increased from the core to the edge of the flow pipe, resulting in lava consolidating gradually from the surface to the core. Maanshan lava is dominated by plane pahoehoe inflated by scoriaceous lava. Heikongshan is characterized by typical scoriaceous lava flow in the proximal phase and the middle phase.

METHODS

Sample Preparation

In this study, a total of eighteen samples were collected from four different volcanoes in the Tengchong volcanic field (Table 1). Six samples were collected from Heikongshan volcano, which covered the northeastern and southwestern parts of the lava field. For the Dayingshan volcano, six samples were collected, parts of which were used to pick zircons for future research (Fig. 8). Four samples were collected from Maanshan volcano. Laoguipo volcano is small and it is difficult to get to the crater, and hence, only two samples were collected (Fig. 9).

In order to analyze the major and trace elements and Hf-Nd isotopes, all the samples we collected were ground in an agate mortar to ~200 mesh at Heibei Geology Academy, Langfang, China. The agate mortar was cleaned with high purity clean sand (SiO_2) powder and 6N pure HCl in an ultrasonic bath for 15 minutes, and then rinsed with ultrapure water. This process was repeated prior to grinding each sample in order to prevent contamination between samples.

P1245 Digital Analytical Balance was used to weigh 200 g powder for each sample in the Institute of Geology and Geophysics, Chinese Academy of Sciences, which were ready for the following geochemical whole-rock and isotope analysis together.

Table 1. Sample collection information gathered using GPS methods in Tengchong volcanic field, SE Tibetan Plateau.

Sample Number	Location	Latitude	Longitude	Altitude (m)	Precision (m)	Remark
HE-1	Heikongshan	N 25°13′39.93″	E 098°29′57.53″	1743	3	two chunks for major and trace elements and Hf-Nd
HE-2	Heikongshan	N 25°12′47.27″	E 098°34′28.20″	1900	3	one chunk for zircon extraction, one chunk for basic geochemical analysis
HE-3	Heikongshan	N 25°15′59.42″	E 098°32′20.63″	1832	2	two chunks for major and trace elements and Hf-Nd
HE-4	Heikongshan	N 25°17′14.01″	E 098°30′22.36″	2037	2	two chunks for major and trace elements and Hf-Nd
HE-5	Heikongshan	N 25°14′19.79″	E 098°30′07.72″	2108	2	two chunks for major and trace elements and Hf-Nd
HE-6	Heikongshan	N 25°13′43.74″	E 098°28′32.55″	1864	2	one chunk for zircon extraction, two chunks for basic geochemical analysis
DA-7	Dayingshan	N 25°08′00.54″	E 098°27′53.22″	1977	2	one chunk for zircon extraction, two chunks for basic geochemical analysis
DA-8	Dayingshan	N 25°06′49.30″	E 098°27′49.02″	2031	2	one chunk for zircon extraction, one chunk for basic geochemical analysis
DA-9	Dayingshan	N 25°07′39.00″	E 098°26′54.69″	2513	2	one chunk for zircon extraction, four chunks for basic geochemical analysis
DA-10	Dayingshan	N 25°08′00.46″	E 098°26′37.16″	2503	2	one chunk for zircon extraction, two chunks for basic geochemical analysis
DA-11	Dayingshan	N 25°08′52.39″	E 098°25′22.10″	1893	2	one chunk for zircon extraction, one chunk for basic geochemical analysis
DA-12	Dayingshan	N 25°09′39.39″	E 098°25′29.32″	1891	2	one chunk for major and trace elements and Hf-Nd
MA-13	Maanshan	N 25°01′20.36″	E 098°25′44.87″	1650	2	one chunk for zircon extraction, two chunks for basic geochemical analysis
LAO-14	Laoguipo	N 25°02′05.33″	E 098°26′47.03″	1794	2	one chunk for zircon extraction, one chunk for basic geochemical analysis
MA-15	Maanshan	N 25°00′04.46″	E 098°25′57.31″	1600	2	one bag for zircon extraction, one bag for basic geochemical analysis
MA-16	Maanshan	N 25°00′34.79″	E 098°24′39.80″	1532	3	one bag for zircon extraction, one bag for basic geochemical analysis
MA-17	Maanshan	N 25°01′38.75″	E 098°23′30.53″	1385	3	one chunk for zircon extraction, one bag for basic geochemical analysis
LAO-18	Laoguipo	N 25°01′36.25″	E 098°26′29.61″	1619	3	one bag for zircon extraction, one bag for basic geochemical analysis

Figure 8. Photographs of volcanic rocks samples collected at Heikongshan and Dayingshan in Tengchong volcanic field, SE Tibetan Plateau (HE: Heikongshan; DA: Dayingshan).

Figure 9. Photographs of volcanic rocks samples collected at Maanshan and Laoguopo in Tengchong volcanic field, SE Tibetan Plateau (MA: Maanshan; LAO: Laoguipo).

Major and Trace Element Analyses

Whole-rock geochemical compositions were measured at the University of Science and Technology of China and commercially ALS Chemex (Guangzhou) Co., Ltd. Major element compositions were determined by X-ray fluorescence (XRF) using fused glass beads. The precision on measured concentrations were typically better than 5% for the major elements. Loss of ignition (LOI) was determined after heating the sample powder to 1,000℃ for one hour. Trace elements were measured by inductively coupled plasma mass spectrometry (ICP-MS) after acid digestion of samples in high-pressure Teflon bombs also at the University of Science and Technology of China and ALS Chemex (Guangzhou) Co., Ltd. Analyses of rock standards verify the precision to be better than 10% for trace and rare earth elements.

Hf Isotope Analyses

Hf isotopes were separated from whole-rock samples and measured at the Institute of Geology and Geophysics, Chinese Academy of Sciences, Beijing, China, directed by a Research Associate. Separation and purification of Hf were carried out on single columns with anion exchange resin following the procedure described in Yang et al. (2007, 2010) and Li et al. (2005).

1. Pre-lab Materials

In this study, Milli-Q water (18.2 MΩ cm^{-1}) from Millipore (Elix-Millipore, USA) and HCl, HNO_3, HF, and $HClO_4$ as twice-distilled ultra-pure grade reagents from Beijing Chemical Factory were used. Hydrochloric acid (6N) was prepared by sub-boiling

distillation in a quartz still. Concentrated nitric and hydrofluoric acid were purified by sub-boiling distillation in a Teflon still. Concentrated perchloric acid was purified by decompressed distillation in a quartz distiller. An international standard solution of ca. 200 μgL^{-1} JMC475 Hf was used for monitoring conditions during the analytical sessions. Standard solutions of 1000 $\mu g\ ml^{-1}$ Hf (Stock No. 14374) purchased from Alfa Aesar of the Johnson Matthey Company (plasma standard solution, Specpure^{TM}) were used to gravimetrically prepare standard solutions with known concentrations. Pre-packed extraction chromatography material (Ln Spec, 100-150 μm particle size, 2 ml) was purchased from Eichrom Industires (Darien IL, USA), while the conventional cation-exchange resin (AG50W-X12, 200-400 mesh size), was obtained from Bio-Rad Inc. (Richmond CA, USA). International Certified Reference Materials (CRMs) rock powders, recommended by the United States Geological Survey (USGS) and the China Geological Survey, were used to evaluate and validate the procedure used.

2. Sample Dissolution

All chemical preparations were conducted on Class 100 work benches inside a Class 1000 clean laboratory at the Institute of Geology and Geophysics, Chinese Academy of Sciences, Beijing, China. About 100 mg of rock powder was weighted into a 7 ml round bottom Savillex^{TM} Teflon screw-top capsule. The concentrate 0.1 ml $HClO_4$ and 2 ml HF were added sequentially to the samples and the capsule capped and then heated on a hotplate at 100-120℃ for one week. The capsule was shaken occasionally during this time in order to dissolve samples completely. After one week, the capsule was opened and then heated the hotplate to 200℃ until no fume going out. 1 ml of 6N HCl

was added to the residue and dried, and this procedure was then repeated. When it had cooled down, the residue was dissolved in 5 ml of 3N HCl. The capsule was again sealed and placed on a hot plate at 80℃ overnight prior to chemical separation.

3. Hf Chemical Separation

The 3N HCl sample solution was centrifuged and then loaded onto pre-conditioned 2 ml Ln Spec resin. Firstly, the matrix elements including Light and Middle Rare Earth Elements (LMREE) were eluted with 3N and 4N HCl sequentially. The Lu (+Yb) fraction was then eluted with 4N HCl. In order to minimize the isobaric interference of ^{176}Lu and ^{176}Yb on ^{176}Hf, the column was rinsed with 6N HCl to effectively remove Lu and Yb residues before collecting the Hf fraction. Photographs and text illustrating the procedure are depicted in Table 2 and Figure 10. After collecting the liquid Hf solution, it was evaporated to dryness and then added to it was 0.1 ml of 2N HF. The sample solution was dried to a little tiny drop and added to 0.8 ml of 2% HNO_3. The mixed solution was transferred to 1.5 ml centrifuge tube and then centrifuged for 10 minutes. Only the top clear solution was transferred to another 1.5 ml centrifuge tube for MC-ICP-MS analysis.

Table 2. Single column procedure for Hf separation using anion exchange chromatography.

Step	Column volumes	Acid
Preparation	20 ml × 3 times	6N HCl + 0.2 N HF
Preconditioning	7 ml × 3 times	3N HCl
Loading samples	5 ml	
Eluting Fe	5 ml × 2 times	3N HCl
Eluting LMREE	5 ml × 2 times	4N HCl
Eluting Lu, Yb	5 ml	4N HCl
Eluting residual Lu, Yb	5 ml × 4 times	6N HCl
Eluting Ti	Variable (50-70 ml for basalt) until elution solution colorless	4N HCl + 0.5% H_2O_2
Collecting Hf	4 ml	2N HF
Cleaning	5 ml	6N HCl
Storing resin		

Source: Modified from Li et al. (2005) and Yang et al. (2007).

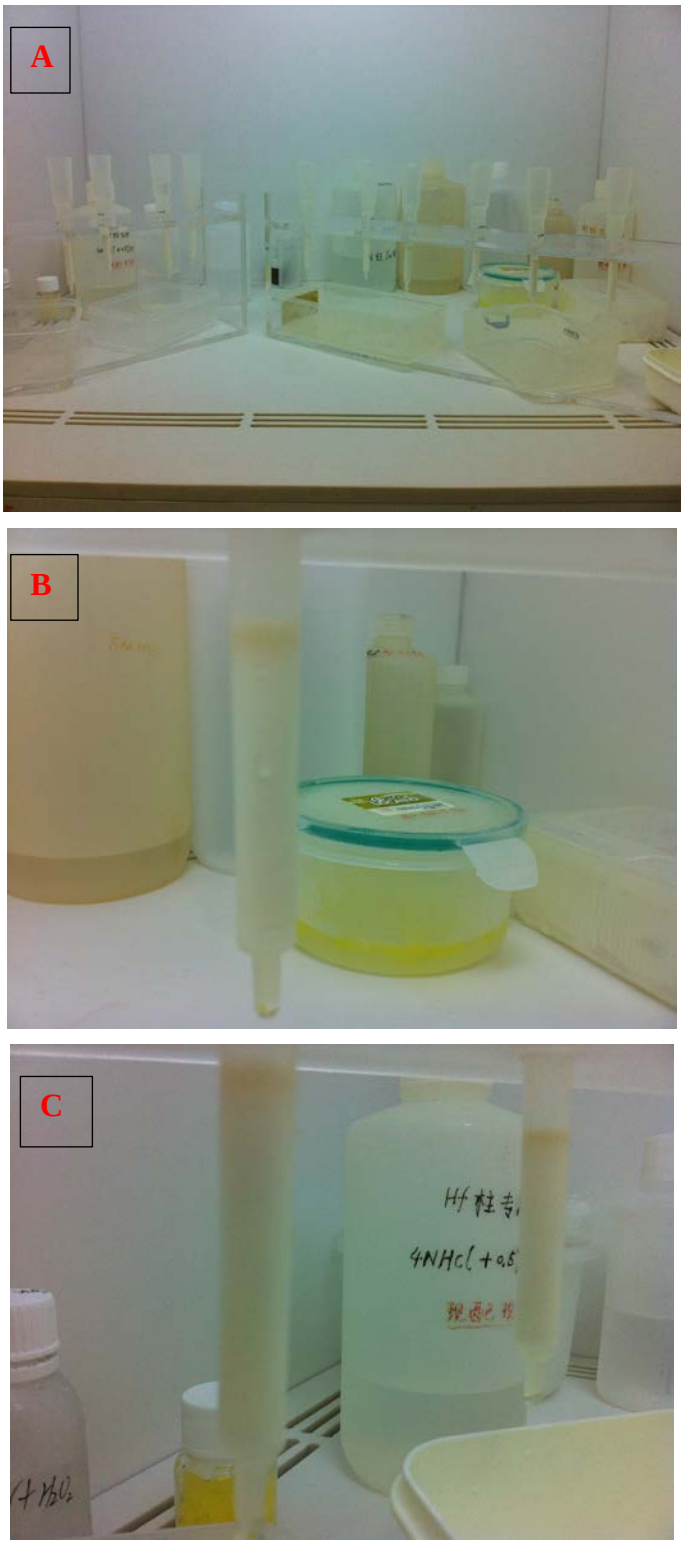

Figure 10. Photographs of the Single Column of Anion Resin Exchange at the Institute of Geology & Geophysics, Chinese Academy of Sciences, China. A. Single column with resin on the holder. B. Liquid Hf in single column. C. Eluting Ti and Fe until the resin changing from red to colorless.

4. Mass Spectrometry

Determination of Hf isotope ratios was carried out in static mode on Faraday cups on the Thermo Fisher Scientific Neptune MC-ICP-MS (Fig. 11). The typical instrument parameters and cup configuration are summarized in Table 3. The Hf fraction was taken up with trace HF and 1 ml of 2% HNO_3. After measurement, 2% HNO_3 and 0.1% HF were used to clean sample injection system before measuring the next sample. It took 10 minutes to complete the measurement of one sample. The time interval between two samples was 5 minutes. Hf isotopic compositions were corrected for mass fractionation bias using $^{179}Hf/^{177}Hf = 0.7325$. Repeated analysis of the reference material was used to monitor the precision, which yielded an average $^{176}Hf/^{177}Hf$ ration of 0.282178 ± 6 (2σ).

Table 3. Typical operating parameters for Lu and Hf measurement.

Neptune MC-ICP-MS	Setting
RF forward power	1300 W
Cooling gas	15.2 l/min
Auxiliary gas	0.6 l/min
Sample gas	~1.10 l/min (optimized daily)
Extraction	−2000 V
Focus	−630 V
Detection system	Nine Faraday collectors
Acceleration voltage	10 kV
Interface cones	Nickel
Spray chamber	Glass cyclonic
Nebulizer type	Micromist PFA nebulizer
Sample uptake rate	50 µl/min
Uptake mode	Free aspiration
Instrument resolution	~400 (low)
Typical sensitivity on ^{180}Hf	~16 V/ppm (10^{-11} Ω resistors)
Sampling mode	9 blocks of 10 cycles for Hf 1 block of 30 cycles for Lu
Integration time	4 s for Hf and 2 s for Lu
Baseline/background determination	*ca.*1 min on peak in 2% HNO_3

Source: From Yang et al. (2010)

Figure 11. Multi-Collector Inductively Coupled Plasma Mass Spectrometer (MC-ICP-MS) at the Institute of Geology & Geophysics, Chinese Academy of Sciences, China.

RESULTS

Whole-Rock Major Element Compositions

The major oxides and trace element compositions of the 18 analyzed rocks from Heikongshan, Dayingshan, Maanshan, and Laoguipo in Tengchong are presented in Tables 4 and 5. The contents of SiO_2 and K_2O in these samples are in the range of 51.39-62.08 wt.% and 1.63-4.18 wt.%, respectively, and the content of Na_2O is relatively constant and close to 3.5 wt.% (Table 4). In the TAS classification diagram (Fig. 12), the youngest Tengchong volcanic rocks range from trachybasalt, basaltic trachyandesite to trachyandesite. The rock type of Heikongshan is mainly basaltic trachyandesite and trachyandesite, and the compositions of these samples are relatively constant, and the contents of SiO_2, CaO, MgO and K_2O are in the range of 51.39-58.69 wt.%, 5.48-8.71 wt.%, 3.72-5.88 wt.%, and 1.63-3.58 wt.%, respectively (Table 4). The rock type of Dayingshan is mainly trachybasalt, and they are characterized by high contents of SiO_2 (58.28-62.08 wt.%) and K_2O (3.69-4.18 wt.%) and low contents of MgO (2.18-2.76 wt.%) and Fe_2O_3 (5.10-6.41 wt.%) (Table 4), which is geochemically different from the other three Holocene volcanoes. The rock type of Maanshan lava is trachyandesite and that for Laoguipo is basaltic trachyandesite. Comparing with other published data, these youngest Tengchong samples span much of the same compositional range as for the entire volcanic field, the exception being the highly evolved older (1 Ma) dacites (Zou et al., 2014).

Table 4. Major element concentrations from Heikongshan, Dayingshan, Maanshan, and Laoguipo in Tengchong.

Sample	HE-1	HE-2	HE-3	HE-4	HE-5	HE-6	DA-7	DA-8	DA-9	DA-10	DA-11	DA-12	MA-13	LAO-14	MA-15	MA-16	MA-17	LAO-18
SiO_2	58.69	51.39	55.38	57.09	58.05	55.15	60.51	60.71	62.08	59.74	59.19	58.28	56.41	53.98	57.44	58.07	58.31	52.06
Al_2O_3	16.33	16.68	17.39	16.82	16.25	16.83	16.01	16.36	15.71	16.36	16.62	16.98	16.96	16.73	16.51	16.71	16.44	16.50
Fe_2O_3	6.23	9.49	6.92	6.63	6.26	7.80	5.67	5.77	5.10	5.97	6.24	6.41	6.88	8.41	6.66	6.58	6.54	9.38
CaO	5.57	8.71	6.67	6.31	5.48	6.74	4.67	4.64	4.14	5.08	5.02	5.08	6.14	6.78	5.70	5.89	5.58	8.01
MgO	3.72	5.88	4.34	4.06	3.74	4.64	2.51	2.50	2.18	2.76	2.65	2.74	3.75	4.82	3.73	3.51	3.56	5.52
Na_2O	3.58	3.64	3.68	3.35	3.56	3.72	3.58	3.57	3.57	3.67	3.61	3.51	3.71	3.31	3.84	3.86	3.76	3.40
K_2O	3.49	1.63	3.07	3.02	3.58	2.73	3.92	3.94	4.18	3.70	3.81	3.69	3.10	2.18	3.41	3.32	3.31	1.82
TiO_2	1.08	1.61	1.27	1.06	1.10	1.24	1.02	1.04	0.91	1.08	1.14	1.17	1.25	1.40	1.21	1.20	1.16	1.56
MnO	0.10	0.16	0.11	0.11	0.11	0.12	0.09	0.09	0.09	0.10	0.10	0.10	0.12	0.13	0.11	0.11	0.11	0.14
P_2O_5	0.43	0.34	0.47	0.31	0.44	0.31	0.39	0.41	0.36	0.44	0.44	0.44	0.49	0.29	0.48	0.46	0.46	0.33
LOI	0.31	0.20	0.22	0.91	1.12	0.20	0.46	0.41	0.60	0.44	0.96	1.05	0.82	1.80	0.29	0.19	0.32	0.44
Total	99.53	99.73	99.52	99.67	99.69	99.48	98.83	99.44	98.92	99.34	99.78	99.45	99.63	99.83	99.38	99.90	99.55	99.16

Table 5. Trace element concentrations from Heikongshan, Dayingshan, Maanshan, and Laoguipo in Tengchong.

Sample	HE-1	HE-2	HE-3	HE-4	HE-5	HE-6	DA-7	DA-8	DA-9	DA-10	DA-11	DA-12	MA-13	LAO-14	MA-15	MA-16	MA-17	LAO-18
Ba	957	312	972	745	938	473	928	1000	898	955	986	1065	832	496	830	809	753	451
Hf	7.8	3.2	6.6	6.1	7.2	4.7	7.7	7.6	7.8	7.5	7.6	8.1	6.1	4.9	6.3	6.3	6.1	3.9
Nb	28.0	18.2	26.3	20.0	27.9	21.2	27.1	28.2	27.6	27.1	27.4	29.6	27.5	19.1	27.7	27.7	26.4	17.2
Ta	1.4	0.8	1.3	1.0	1.4	1.1	1.5	1.5	1.5	1.4	1.4	1.5	1.4	1.0	1.4	1.4	1.4	0.9
Pb	21.6	5.1	17.2	19.4	21.8	13.9	26.2	24.9	28.4	26.5	26.0	29.2	19.8	16.2	19.8	19.0	19.8	10.2
Th	26.1	5.7	20.7	30.7	25.1	21.6	33.4	32.7	40.2	29.1	31.0	34.1	21.3	24.8	24.6	24.1	24.5	13.6
U	2.57	0.69	2.27	2.54	2.55	2.02	3.15	3.05	3.48	2.70	2.75	2.95	2.32	2.29	2.61	2.63	2.56	1.36
Y	26.4	22.8	24.9	23.5	25.6	24.9	27.2	28.3	27.3	27.0	31.1	30.3	26.9	26.3	26.8	27.3	25.9	25.3
Zr	327	139	291	250	317	205	313	322	320	316	322	348	270	194	270	273	258	168
Cr	48	122	33	55	45	71	16	19	15	22	13	12	61	116	62	54	58	126
Cs	1.21	0.29	0.82	1.09	1.12	0.94	1.74	1.48	2.13	1.59	1.56	1.55	1.15	0.99	1.54	1.61	1.52	0.78
Ga	20.30	19.70	20.80	19.85	19.85	18.75	20.70	20.60	21.00	21.90	21.30	23.60	21.10	20.20	20.80	21.20	19.65	19.85
Rb	109.0	27.1	84.4	102.0	107.0	80.7	132.0	131.5	151.5	115.5	116.5	110.0	83.2	65.6	102.0	101.0	99.3	46.1
Sn	2.0	2.0	2.0	2.0	2.0	2.0	3.0	2.0	3.0	3.0	2.0	3.0	2.0	3.0	2.0	2.0	2.0	2.0
Sr	534	423	646	552	518	441	466	488	427	505	502	544	593	397	588	580	537	449
V	105	164	125	118	102	131	90	92	79	93	102	110	115	132	110	113	104	153
La	74.6	21.5	69.2	65.9	72.9	43.3	79.2	81.4	82.9	76.7	90.6	90.5	64.4	45.2	66.6	66.8	64.6	33.8
Ce	144.0	43.0	133.0	129.5	140.0	83.6	152.5	152.5	160.5	147.0	160.5	172.0	121.5	88.3	126.0	126.0	123.0	66.5
Pr	15.05	4.89	14.10	13.95	14.75	9.16	16.05	16.65	16.95	15.65	17.65	18.30	12.80	9.68	13.10	13.40	13.00	7.35
Nd	54.6	20.8	52.1	50.5	53.3	33.4	58.2	59.7	59.6	56.1	64.5	64.4	47.4	35.1	49.2	49.1	47.1	28.5
Sm	8.79	4.76	8.75	8.43	8.63	6.09	9.33	9.13	9.92	9.00	10.50	10.55	8.17	6.62	8.71	8.30	8.11	6.09
Eu	1.79	1.49	1.85	1.67	1.81	1.36	1.74	1.84	1.60	1.81	1.94	2.04	1.76	1.51	1.77	1.79	1.67	1.55
Gd	6.83	4.77	6.45	6.13	6.40	5.45	6.70	7.27	7.10	7.14	7.85	7.91	6.27	5.99	6.54	6.46	6.39	5.56
Tb	1.01	0.77	0.98	0.87	0.96	0.86	1.04	1.00	1.01	1.05	1.08	1.13	0.96	0.90	0.99	0.95	0.90	0.82
Dy	5.41	4.40	5.13	4.81	5.27	4.98	5.50	5.73	5.79	5.54	6.42	6.15	5.29	5.27	5.53	5.53	5.28	5.08
Ho	1.02	0.91	1.00	0.94	1.01	0.98	1.01	1.11	1.06	1.09	1.19	1.24	0.99	1.01	1.07	1.06	1.03	0.99
Er	3.05	2.46	2.58	2.57	2.78	2.88	2.81	3.24	2.87	2.97	3.17	3.35	2.99	2.98	2.93	3.05	2.93	2.84
Tm	0.38	0.31	0.36	0.35	0.34	0.40	0.39	0.40	0.38	0.41	0.45	0.39	0.40	0.42	0.37	0.41	0.35	0.35
Yb	2.40	2.12	2.21	2.04	2.26	2.36	2.61	2.63	2.53	2.62	2.61	2.79	2.47	2.45	2.61	2.64	2.48	2.24
Lu	0.34	0.32	0.32	0.34	0.38	0.37	0.35	0.40	0.39	0.38	0.44	0.40	0.39	0.35	0.42	0.39	0.37	0.34
ΣREE	319.27	112.50	298.03	288.00	310.79	195.19	337.43	343.00	352.60	327.46	368.90	381.15	275.79	205.78	285.84	285.88	277.21	162.01
LREE	298.83	96.44	279.00	269.95	291.39	176.91	317.02	321.22	331.47	306.26	345.69	357.79	256.03	186.41	265.38	265.39	257.48	143.79
HREE	20.44	16.06	19.03	18.05	19.40	18.28	20.41	21.78	21.13	21.20	23.21	23.36	19.76	19.37	20.46	20.49	19.73	18.22
LREE/HREE	14.62	6.00	14.66	14.96	15.02	9.68	15.53	14.75	15.69	14.45	14.89	15.32	12.96	9.62	12.97	12.95	13.05	7.89
La_N/Yb_N	22.30	7.27	22.46	23.17	23.14	13.16	21.77	22.20	23.50	21.00	24.90	23.27	18.70	13.23	18.30	18.15	18.68	10.82
δEu	0.68	0.95	0.72	0.68	0.71	0.71	0.64	0.67	0.56	0.67	0.63	0.65	0.72	0.72	0.69	0.72	0.68	0.80
δCe	0.99	0.99	0.99	1.00	0.99	0.98	0.99	0.96	0.99	0.98	0.92	0.98	0.98	0.99	0.98	0.97	0.98	0.99

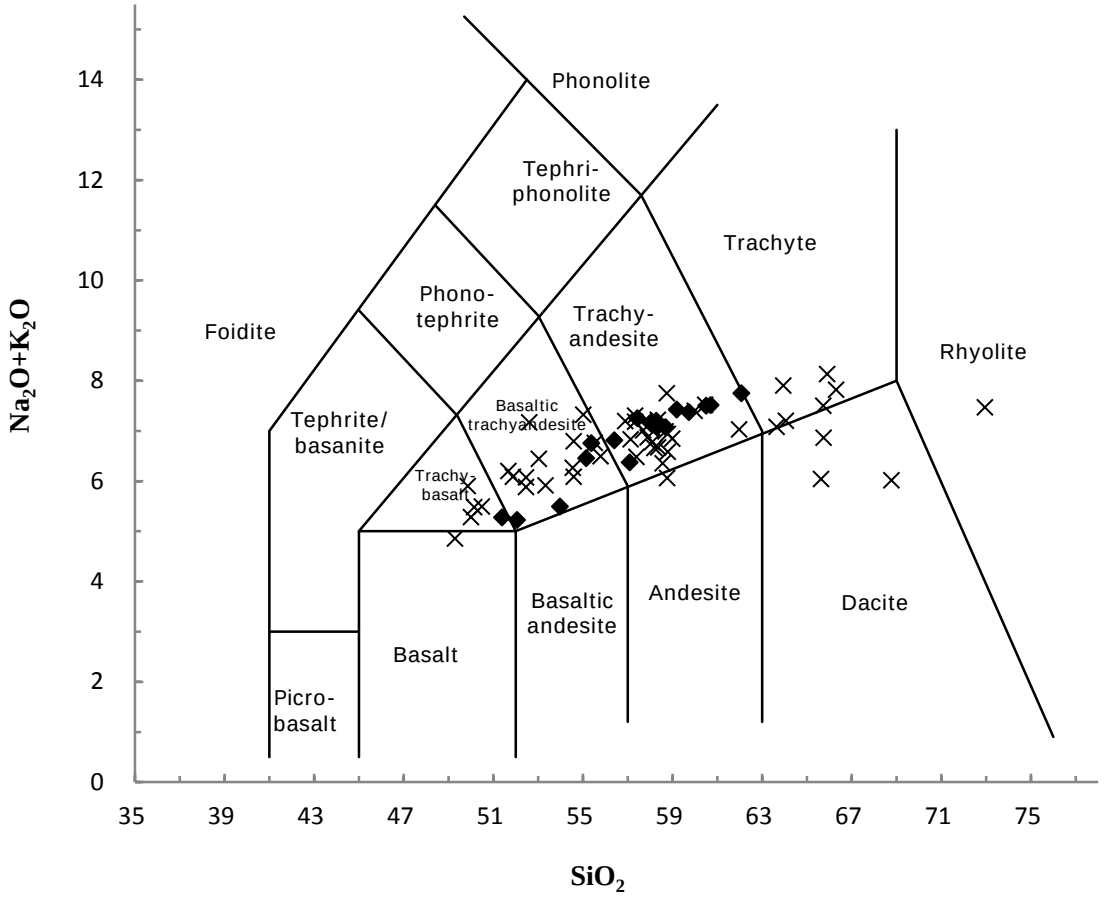

Figure 12. Total Alkalis-Silica (TAS) diagram for the volcanic rocks from Tengchong. Black diamond denotes samples from Heikongshan, Dayingshan, Maanshan, and Laoguipo (this study). Black cross denotes data from other published Tengchong volcanic rocks (Chen et al., 2006; Yu et al., 2010; Zhao and Fan, 2010; Zhou et al., 2012).

In the AFM diagram (Fig. 13), all samples including the 18 samples analyzed in the current study and other published data in Tengchong show a clear calc-alkaline trend. In the K_2O-SiO_2 diagram (Fig. 14) and the K_2O-Na_2O diagram (Fig. 15), all of the rocks have higher Na_2O than K_2O and plot on the boundary between the high-K calc-alkaline and shoshonitic fields, which is different from much of the volcanism on the main parts of the Tibetan Plateau. Therefore, the compositional characteristics illustrate that the major element concentration of the eruption products between the four Tengchong Holocene volcanoes (Heikongshan, Dayingshan, Maanshan, and Laoguipo) show apparent differences. K_2O has a well-defined positive correlation with SiO_2. The rocks established already are significantly enriched in P_2O_5 and form a distinct trend in Harker plots (Fig. 16). Al_2O_3, MgO, Fe_2O_3, CaO, and TiO_2 show moderately good negative correlations with SiO_2, while K_2O has good positive one (Figs. 16 and 17). These chemical variations can be interpreted in terms of fractional crystallization processes (Wilson, 1989). The Tengchong volcanic rocks, therefore, share evolutionary relationships with the four youngest volcanoes. The evolution degree of volcanics composition has been enhanced from Laoguipo, Maanshan, Heikongshan to Dayingshan, which is consistent with previous studies (Zhao and Fan, 2010).

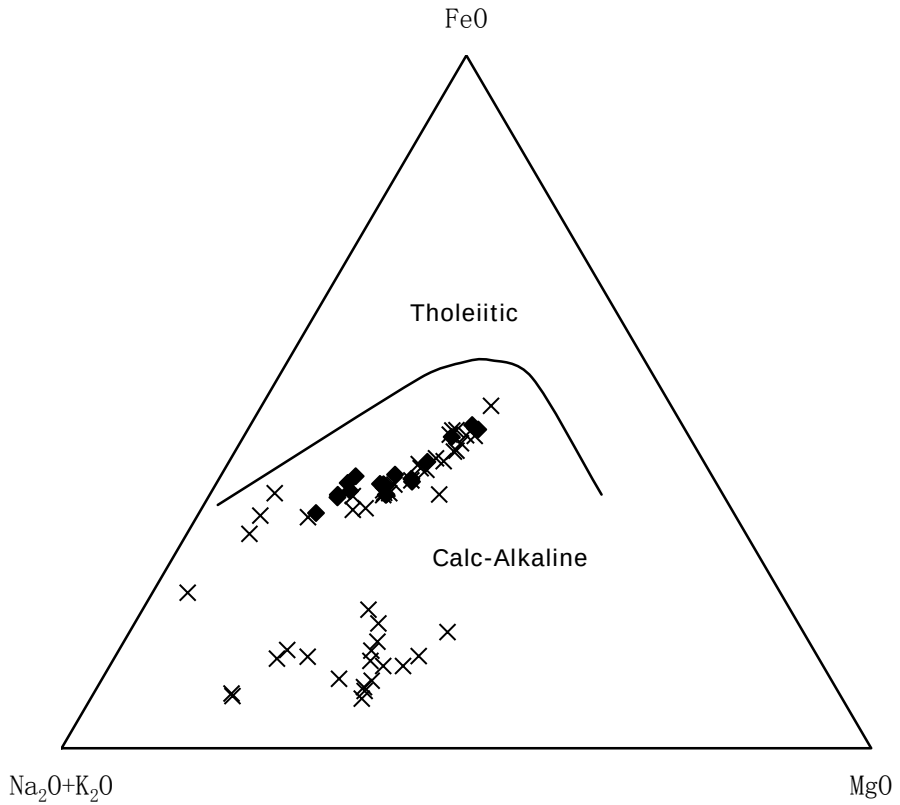

Figure 13. Alkalis-Fe-Mg (AFM) diagram for the volcanic rocks from Tengchong. Black diamond denotes samples from Heikongshan, Dayingshan, Maanshan, and Laoguipo (this study). Black cross denotes data from other published Tengchong volcanic rocks (Chen et al., 2006; Yu et al., 2010; Zhao and Fan, 2010; Zhou et al., 2012).

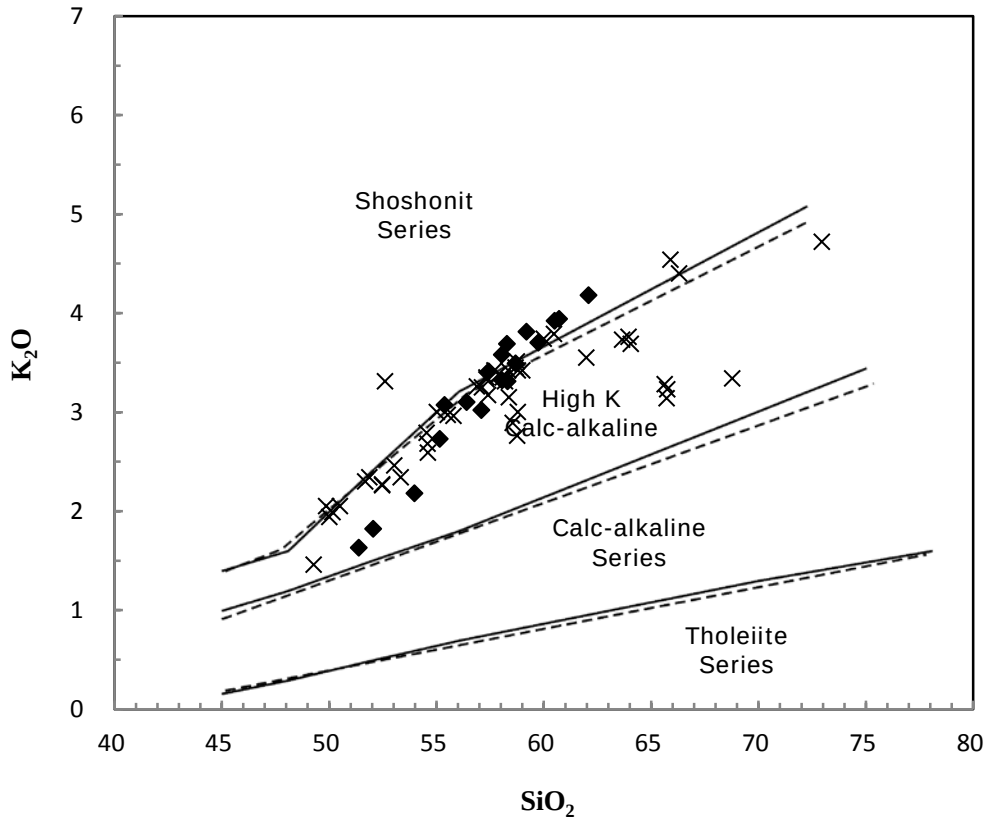

Figure 14. K_2O versus SiO_2 diagram for Tengchong volcanic rocks. Black diamond denotes samples from Heikongshan, Dayingshan, Maanshan, and Laoguipo (this study). Black cross denotes data from other published Tengchong volcanic rocks (Chen et al., 2006; Yu et al., 2010; Zhao and Fan, 2010; Zhou et al., 2012).

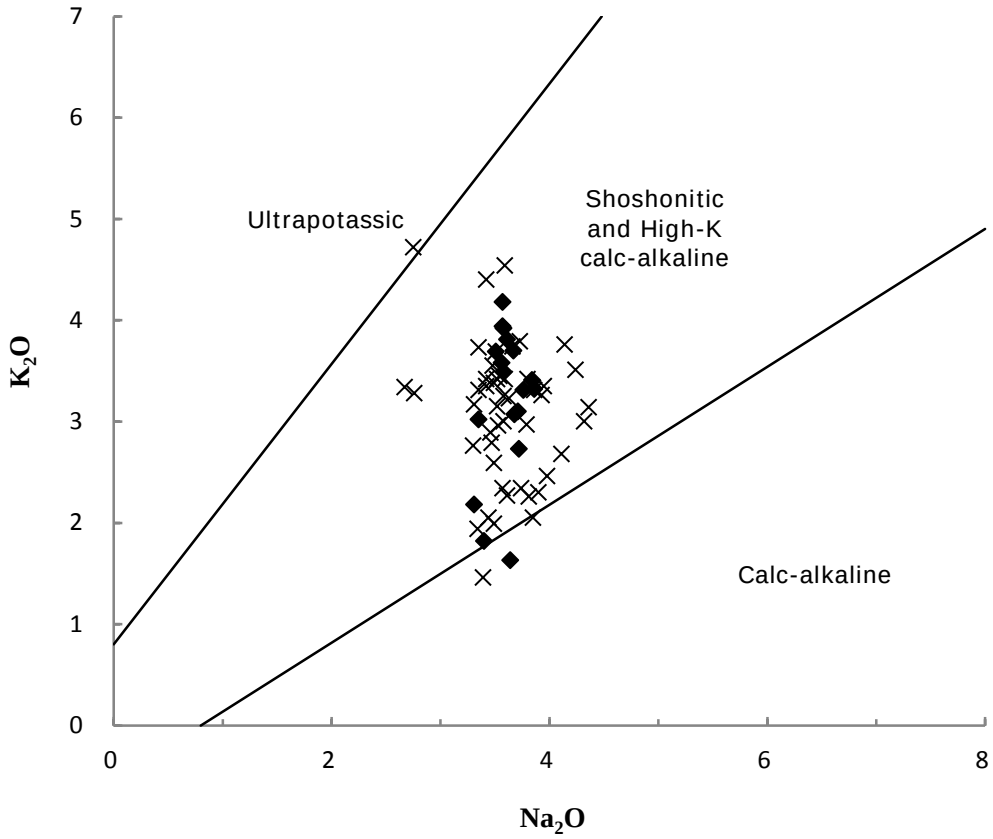

Figure 15. Na_2O versus K_2O diagram for the volcanic rocks in Tengchong. Black diamond denotes samples from Heikongshan, Dayingshan, Maanshan, and Laoguipo (this study). Black cross denotes data from other published Tengchong volcanic rocks (Chen et al., 2006; Yu et al., 2010; Zhao and Fan, 2010; Zhou et al., 2012).

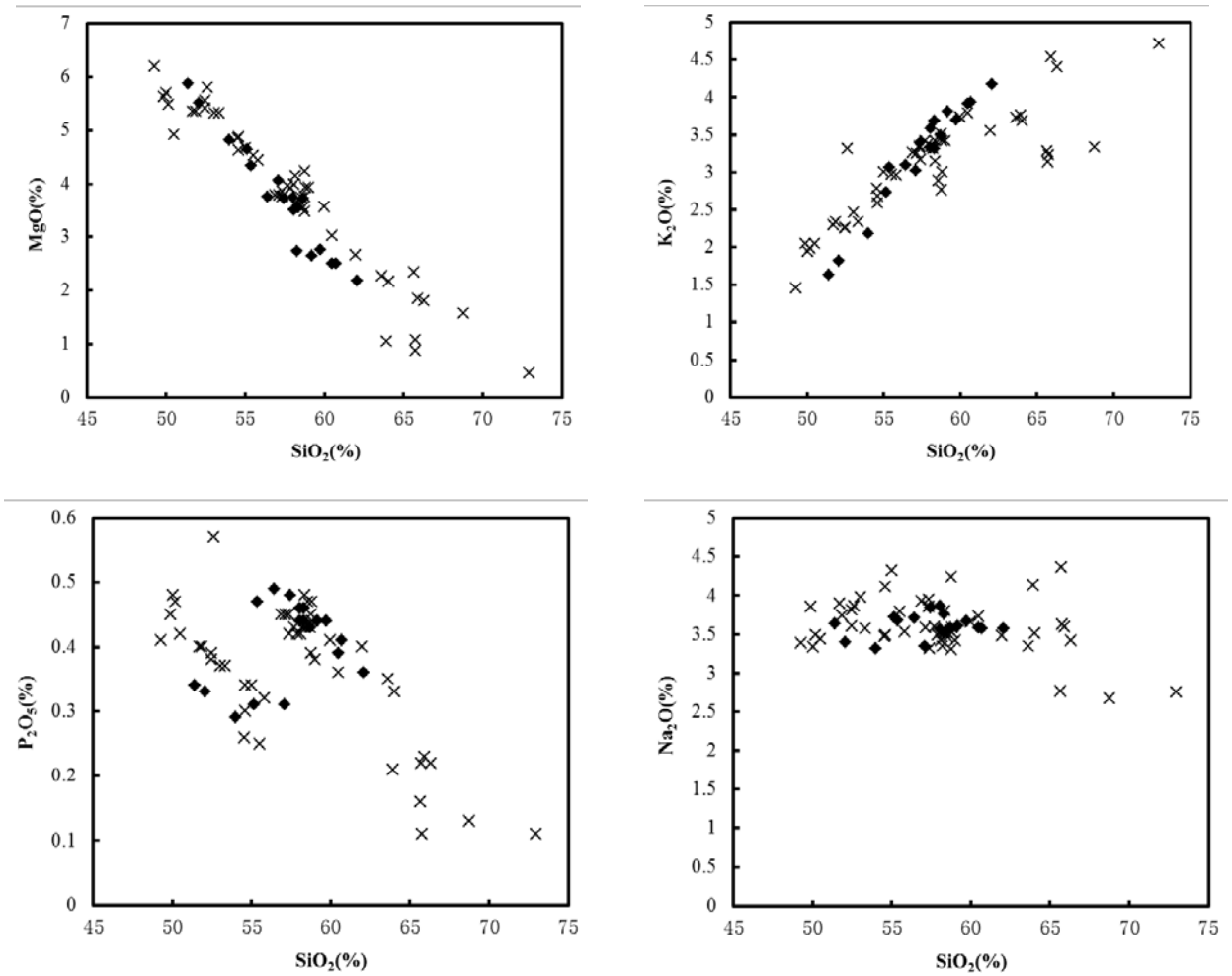

Figure 16. Harker Diagram of MgO, K_2O, P_2O_5, and Na_2O vs. SiO_2 for Tengchong volcanic rocks. Black diamond denotes samples from Heikongshan, Dayingshan, Maanshan, and Laoguipo (this study). Black cross denotes data from other published Tengchong volcanic rocks (Chen et al., 2006; Yu et al., 2010; Zhao and Fan, 2010; Zhou et al., 2012).

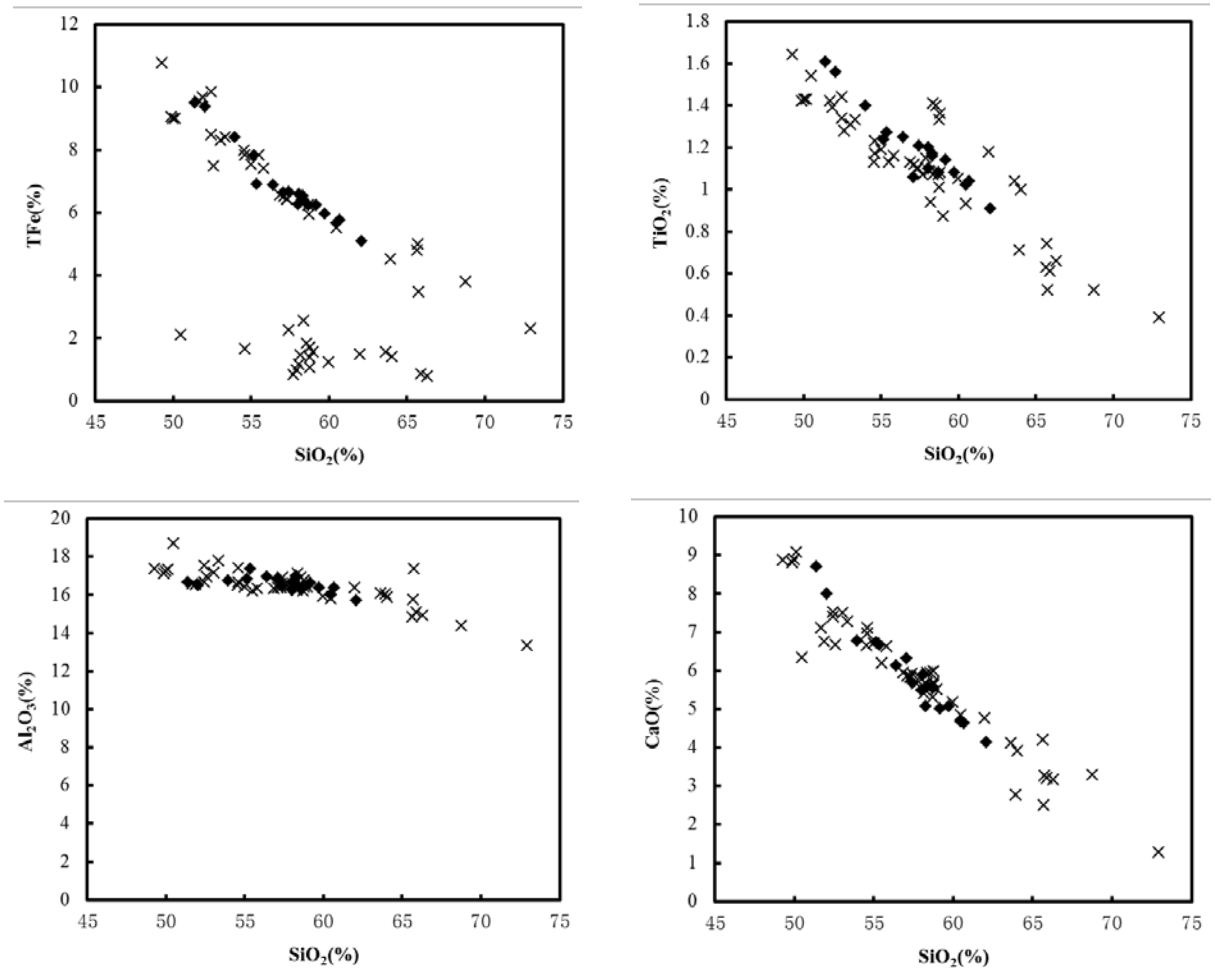

Figure 17. Harker Diagram of FeO, TiO_2, Al_2O_3, and CaO vs. SiO_2 for Tengchong volcanic rocks. Black diamond denotes samples from Heikongshan, Dayingshan, Maanshan, and Laoguipo (this study). Black cross denotes data from other published Tengchong volcanic rocks (Chen et al., 2006; Yu et al., 2010; Zhao and Fan, 2010; Zhou et al., 2012).

Whole-Rock Trace Element Compositions

The Tengchong samples are enriched in incompatible elements. Figures 18-23 present the Chondrite-normalized REE patterns of the Dayingshan, Heikongshan, Maanshan, and Laoguipo volcanic rocks. Among all the samples, Dayingshan has the highest ∑ REE and the lowest δEu, where ∑ REE = $327.46 \times 10^{-6} \sim 381.15 \times 10^{-6}$, δEu = 0.56 ~ 0.67, and $(La/Yb)_N$ is 21.00 ~ 24.90. In contrast, Laoguipo has the lowest ∑ REE and the highest δEu, where ∑ REE = $162.01 \times 10^{-6} \sim 205.78 \times 10^{-6}$, δEu = 0.72 ~ 0.79, and $(La/Yb)_N$ is 10.82 ~ 13.23. Maanshan and Heikongshan have ∑ REE values between the other two volcanoes. For Maanshan, they are ∑ REE = $275.79 \times 10^{-6} \sim 285.88 \times 10^{-6}$, δEu = 0.68 ~ 0.72, and $(La/Yb)_N$ is 18.15 ~ 18.70. For Heikongshan, ∑ REE = $112.50 \times 10^{-6} \sim 319.27 \times 10^{-6}$, δEu = 0.68 ~ 0.95, and $(La/Yb)_N$ is 7.27 ~ 23.17 (Table 5). In the Chondrite-normalized REE patterns, all the samples show LREE enrichment over HREE and moderate negative Eu anomalies (Figs. 18 through 23). Igneous rock REE patterns are controlled by source rock REE geochemistry and mineral-melt partitioning during magmatic evolution. Negative Eu anomalies are mainly controlled by plagioclase. Since rocks in this area have high plagioclase content, plagioclase was separated from the felsic magma during the fractional crystallization or was left in the mantle source region during the partial melting process, leading to negative Eu anomalies in lava. Significant LREE enrichment relative to HREE and negative ε_{Nd} values suggest that the source is an enriched mantle.

Trace element geochemistry of these four eruptive events is similar overall (Table 5), indicating high enrichment in Large Ion Lithophile Elements (LILE) and depletion of High Field Strength Elements (HFSE). Figures 24-29 present the trace element spider

diagram of the Dayingshan, Heikongshan, Maanshan, and Laoguipo volcanic rocks. All studied samples have positive anomalies in Rb, Th, U, K, Pb, and Nd, and negative anomalies in Nb, Ta, Sr, P, and Ti, especially with obvious negative Nb, Ta anomalies, suggesting that they may have characteristics of island arc or active continental margin volcanics. The four volcanoes share similarities with the volcanoes of typical island arcs or continental margins formed around the world, which indicates that oceanic crust material is involved in the origin of the Tengchong magma (Zhao and Fan, 2010). Since Nb and Ta levels are relatively low in subduction-related hydrous fluids or sediment melts, the negative Nb and Ta anomalies may result from partial melting of a mantle source metasomatized by hydrous fluids or sediment melts from the subducting plate. In addition, the negative Sr anomalies may result from the fractional crystallization of plagioclase (Wilson, 1989). From Laoguipo, Maanshan, Heikongshan to Dayingshan, the average content of incompatible elements in Rb, Th, U, Pb, etc. gradually increase. However, the average content of high field strength elements such as Nb, Ta, etc. does not have an obvious trend. In addition, Dayingshan has the lowest Cr content, while Laoguipo has the highest value, which could be interpreted to correlate lower Cr content with higher magma evolution grade (Figs. 24 through 29). The extremely similar REE and trace element patterns of the volcanics among those four youngest volcanoes may reflect the homogeneous initial phases of magma.

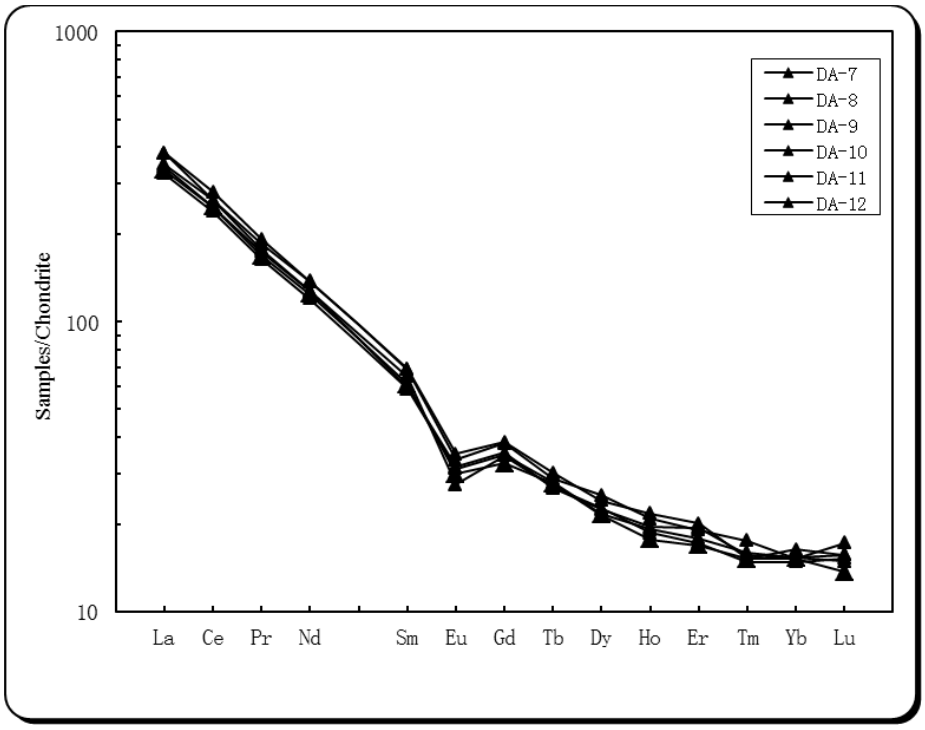

Figure 18. Chondrite-normalized REE patterns of the Dayingshan volcanic rocks. Chondrite-normalized values are from Nakamurma (1974).

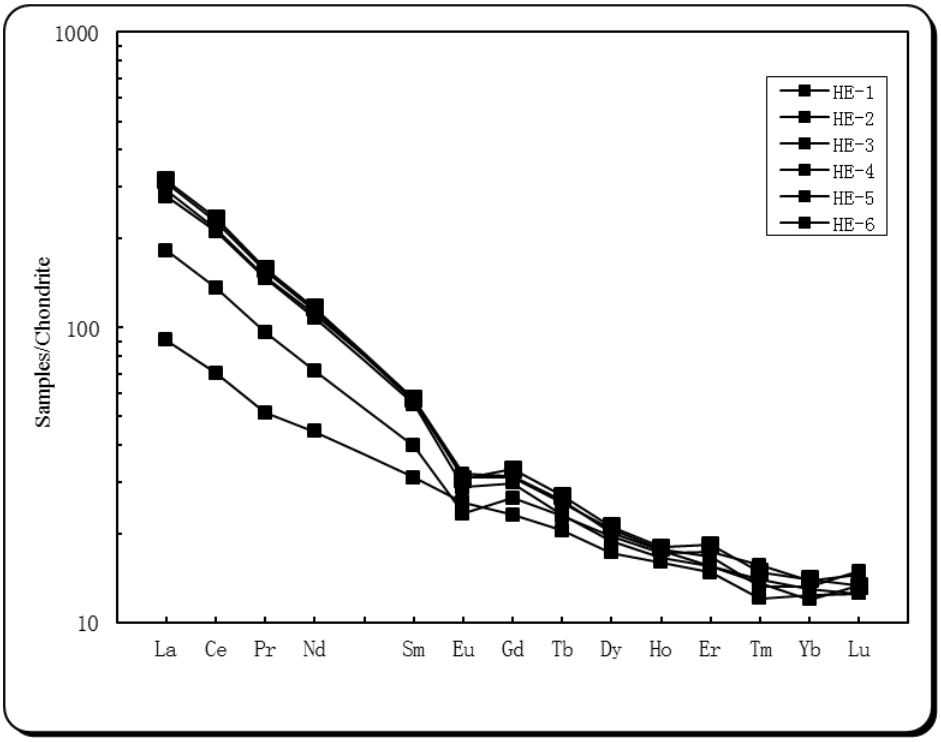

Figure 19. Chondrite-normalized REE patterns of the Heikongshan volcanic rocks. Chondrite-normalized values are from Nakamurma (1974).

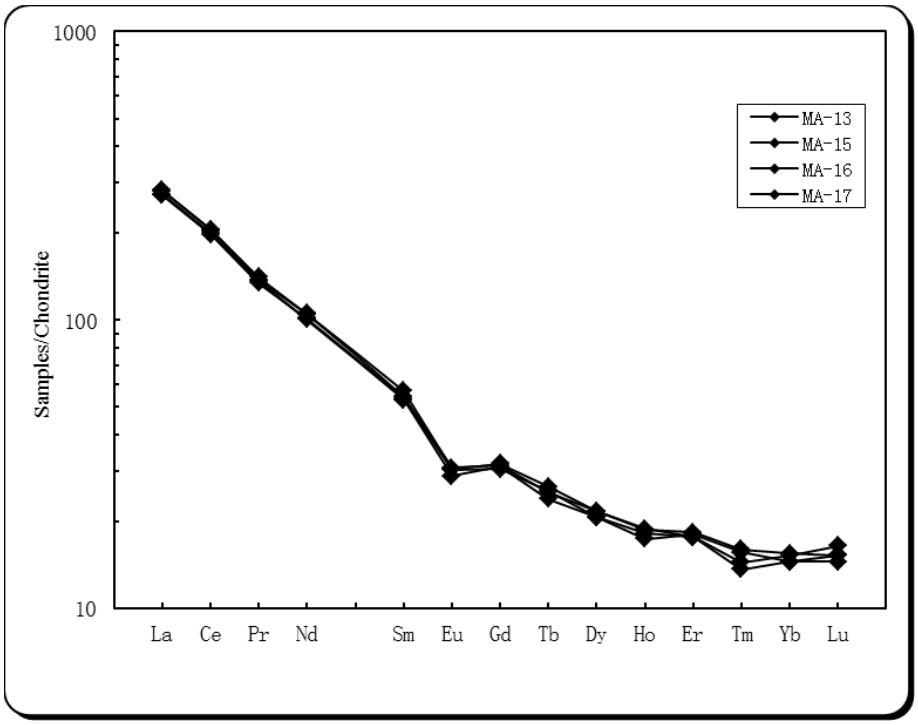

Figure 20. Chondrite-normalized REE patterns of the Maanshan volcanic rocks. Chondrite-normalized values are from Nakamurma (1974).

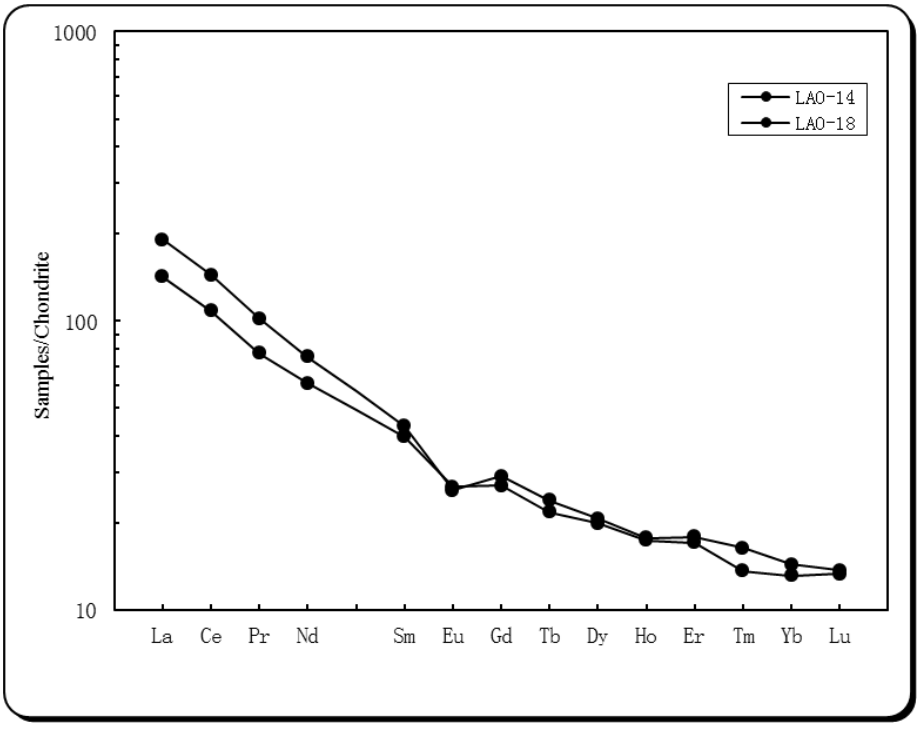

Figure 21. Chondrite-normalized REE patterns of the Laoguipo volcanic rocks. Chondrite-normalized values are from Nakamurma (1974).

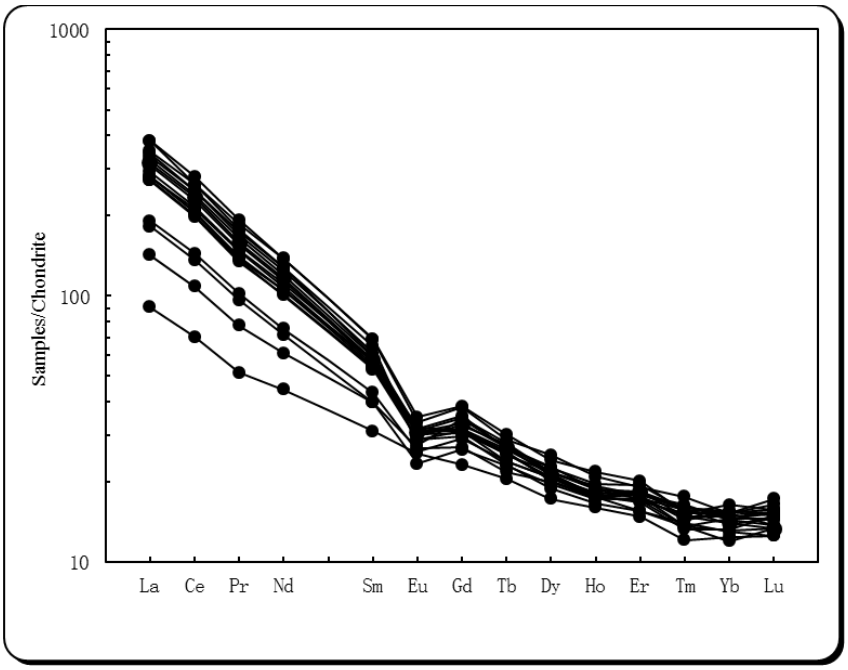

Figure 22. Chondrite-normalized REE patterns of the Heikongshan, Dayingshan, Maanshan, and Laoguipo volcanic rocks in Tengchong. Chondrite-normalized values are from Nakamurma (1974).

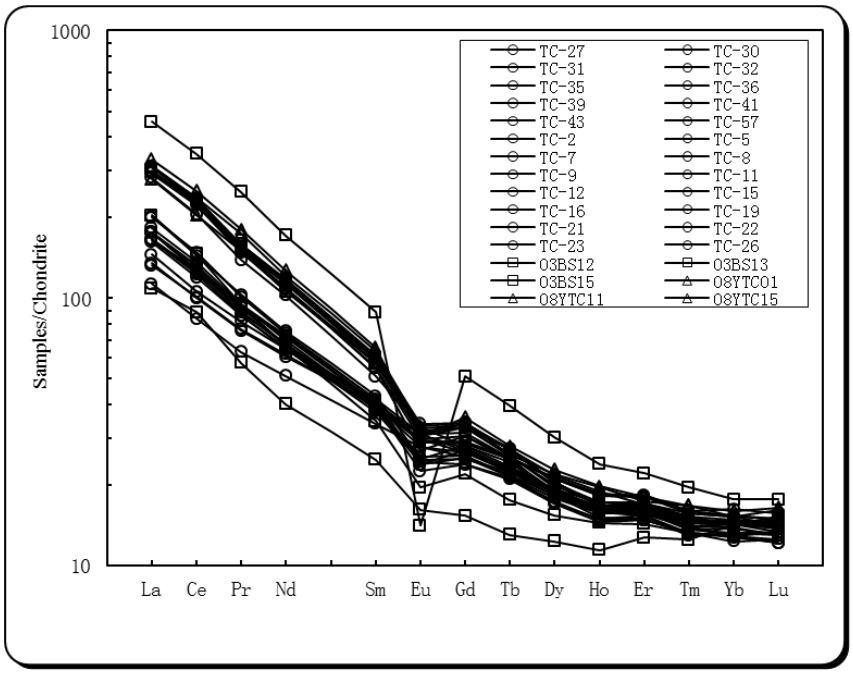

Figure 23. Chondrite-normalized REE patterns of Tengchong volcanic rocks. Data sources for other published Tengchong volcanic rocks: Chen et al. (2006), Zhao and Fan (2010), Zhou et al. (2012).Chondrite-normalized values are from Nakamurma (1974).

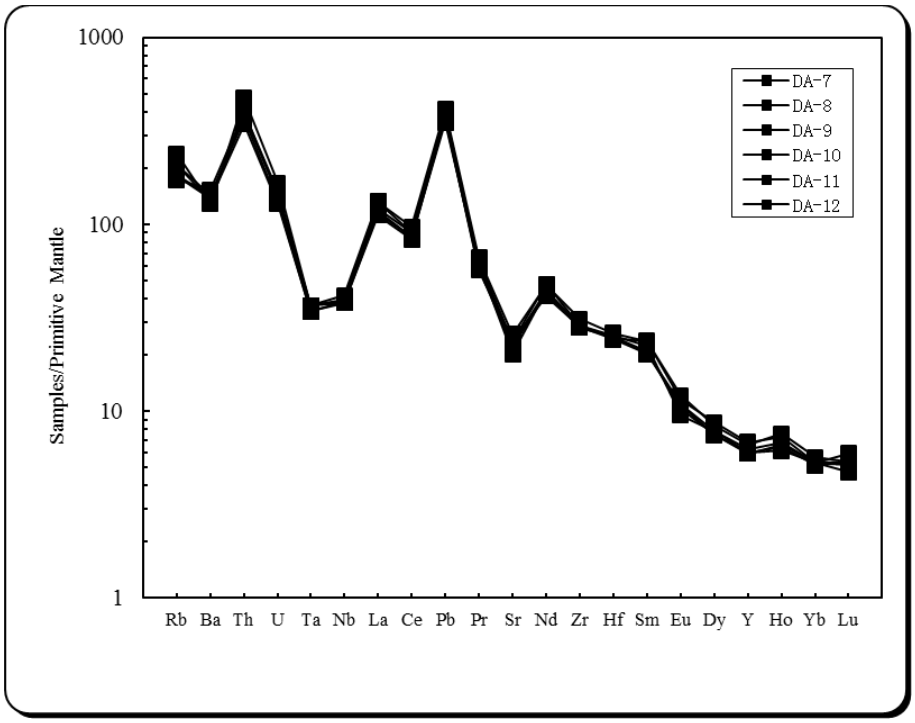

Figure 24. Trace element spider diagram of the Dayingshan volcanic rocks. Primitive mantle-normalized values are from McDonough and Sun (1995).

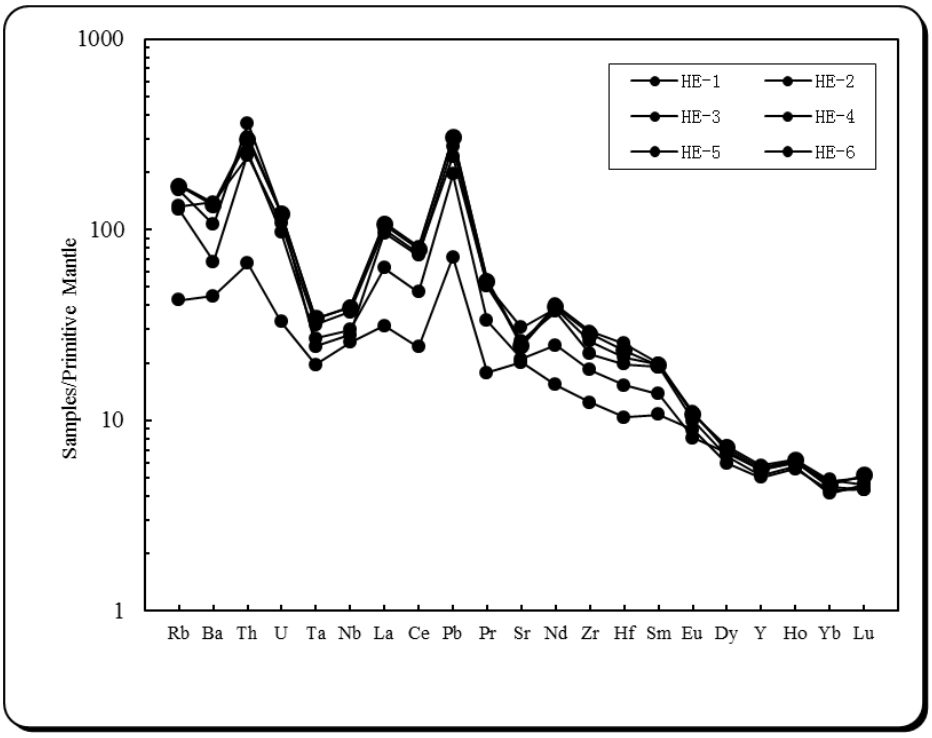

Figure 25. Trace element spider diagram of the Heikongshan volcanic rocks. Primitive mantle-normalized values are from McDonough and Sun (1995).

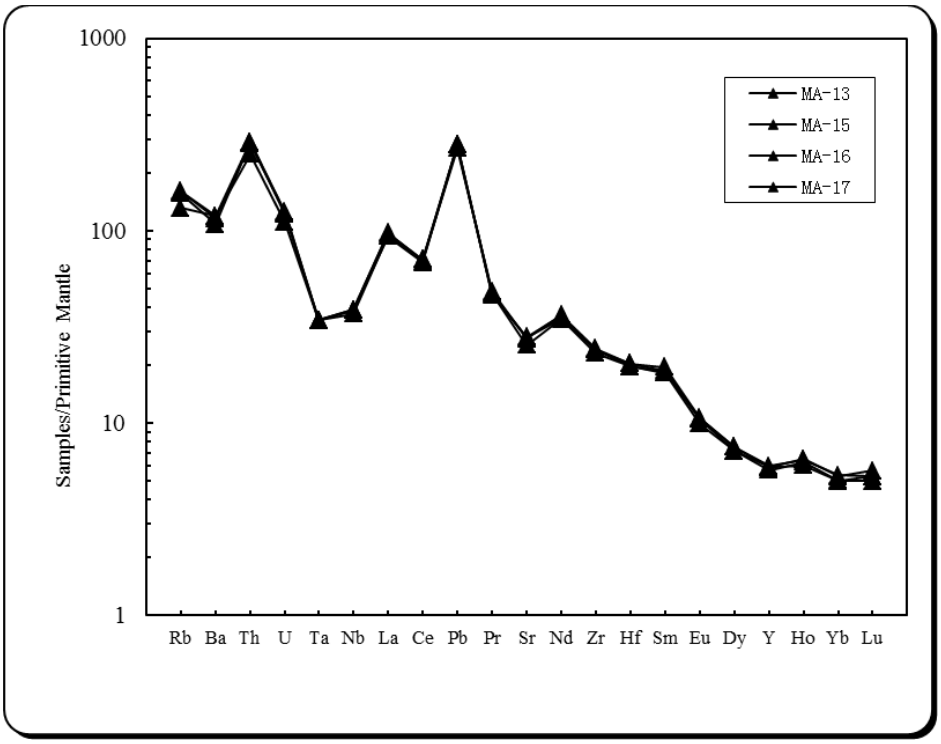

Figure 26. Trace element spider diagram of the Maanshan volcanic rocks. Primitive mantle-normalized values are from McDonough and Sun (1995).

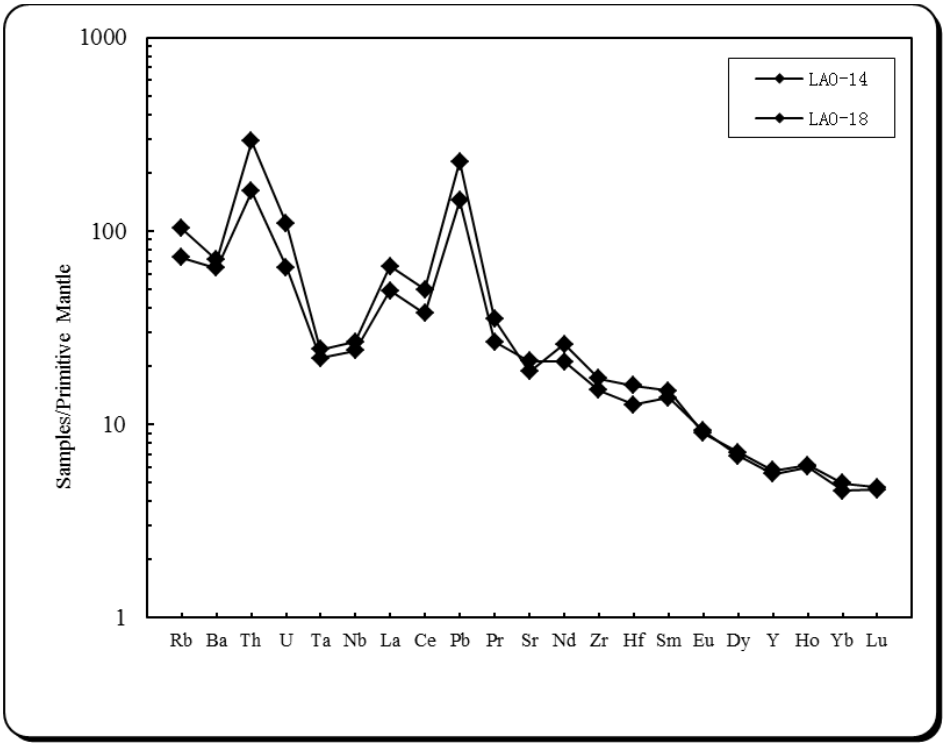

Figure 27. Trace element spider diagram of the Laoguipo volcanic rocks. Primitive mantle-normalized values are from McDonough and Sun (1995).

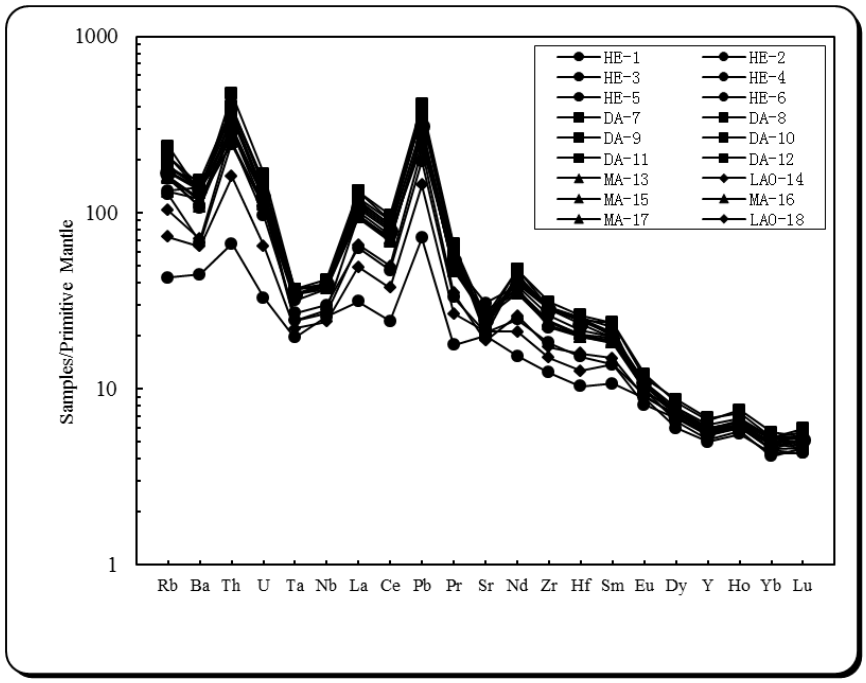

Figure 28. Trace element spider diagram of the Heikongshan, Dayingshan, Maanshan, and Laoguipo volcanic rocks in Tengchong. Primitive mantle-normalized values are from McDonough and Sun (1995).

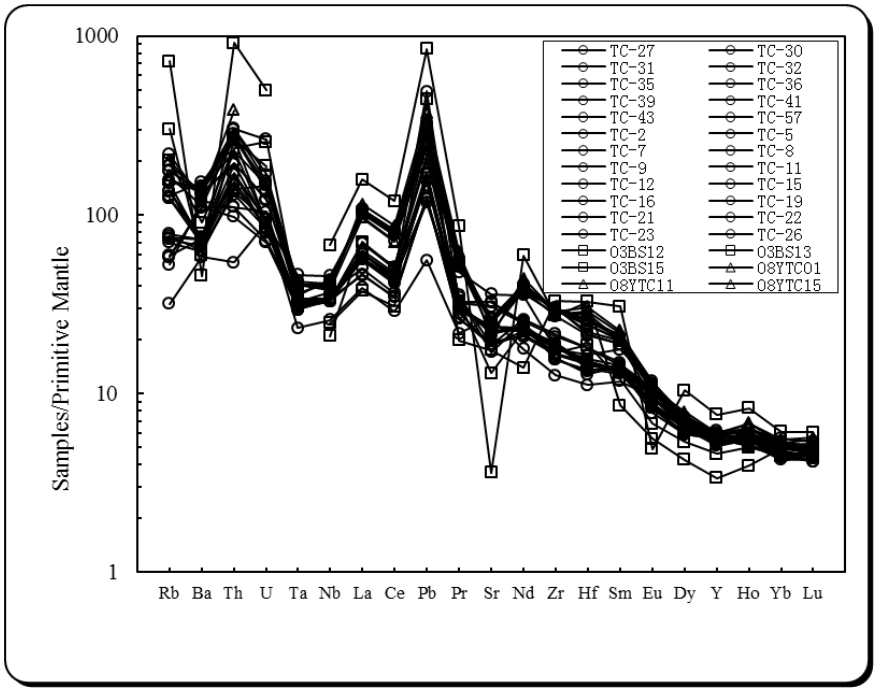

Figure 29. Trace element spider diagram of Tengchong volcanic rocks. Data sources for other published Tengchong volcanic rocks: Chen et al. (2006), Zhao and Fan (2010), Zhou et al. (2012). Primitive mantle-normalized values are from McDonough and Sun (1995).

Whole-Rock Hf Isotopes

The Hf isotopic data of 18 samples from Heikongshan, Dayingshan, Maanshan, and Laoguipo in Tengchong are depicted in Table 6. These samples have $^{176}Hf/^{177}Hf$ ratios of 0.282563~0.282993. The rocks from Laoguipo have higher $^{176}Hf/^{177}Hf$ values ranging from 0.282761~0.282839, with ε_{Hf} values from -0.7 to -3.5, whereas Dayingshan has lower values ranging from 0.282563~0.282653, with ε_{Hf} from -7.3 to -10.5. The Hf data from Maanshan have redundant less variation (ε_{Hf} from -6.0 to -6.6) than the other volcanoes. In contrast, Hf isotopic compositions for Heikongshan samples exhibit significant variations (ε_{Hf} from -10.3 to 4.7). Only one sample from Heikongshan shows positive ε_{Hf} value, all other samples have negative ε_{Hf} values, which means they are caused by a deficiency of ^{176}Hf and imply derivation from a source with a lower Lu/Hf ratio than the chondritic reservoir (Faure and Mensing, 2005).

Table 6. Hf isotopes of representative lavas from Heikongshan, Dayingshan, Maanshan, and Laoguipo in Tengchong.

Sample	$^{176}Hf/^{177}Hf$	$2\sigma_m$	εHf
HE-1	0.282595	9	-9.4
HE-2	0.282993	13	4.7
HE-3	0.282597	7	-9.3
HE-4	0.282567	10	-10.3
HE-5	0.282607	6	-8.9
HE-6	0.282823	9	-1.3
DA-7	0.282589	8	-9.6
DA-8	0.282571	8	-10.2
DA-9	0.282563	9	-10.5
DA-10	0.282576	7	-10.0
DA-11	0.282603	11	-9.1
DA-12	0.282653	8	-7.3
MA-13	0.282689	6	-6.1
LAO-14	0.282761	7	-3.5
MA-15	0.282691	7	-6.0
MA-16	0.282673	5	-6.6
MA-17	0.282673	6	-6.6
LAO-18	0.282839	7	-0.7

DISCUSSION

Magma Origin and Evolution

Major and trace element concentration and isotopic composition analyses indicate that the Tengchong volcanic rocks in Heikongshan, Dayingshan, Maanshan, and Laoguipo volcanoes were derived from an enriched mantle. The onset of melting beneath Tengchong is linked to recent fluid fluxing in the mantle wedge. Lavas from the four youngest volcanoes erupted through thick continental crust rather than thin oceanic crust, which are consistent with the influence of the thickness of the overlying lithosphere on the mantle dynamics and partial melting within the wedge (Zou et al., 2010). The chemical and isotopic data show that the main series lavas were derived by partial melting of a metasomatized and heterogeneous mantle source, with crustal and possibly seawater components related to prior subduction beneath Asia after the collision (Zhu et al., 1983).

Previous studies (Zhu et al., 1983; Fan et al., 2001; Zhao and Fan, 2010) considered that P and Ti negative anomalies may indicate the crystal fractionation of pyroxene, titanium oxide and apatite, while Sr and Eu negative anomalies may relate to fractional crystallization of plagioclase. This would suggest that the Tengchong Holocene volcanic magma evolved from pyroxene, titanium oxide and apatite crystal fractionation in the early stages, and plagioclase fractional crystallization playing a more important role during magma ascension. Comparing the major elements, REEs, and incompatible trace elements from the four youngest volcanoes, the magmas beneath Heikongshan, Dayingshan, Maanshan, and Laoguipo have the homogeneous characteristics, but experienced different degrees of fractional crystallization to evolve from trachybasalt to

basaltic trachyandesite to trachyandesite, which tracks the basic to the acidic volcanic combinations.

Sr-Nd Mantle Character

The Tengchong samples have high $^{87}Sr/^{86}Sr$ and low $^{143}Nd/^{144}Nd$ (Fig. 30). Their ε_{Nd} varies from -4.4 to -10.1, showing enriched characteristics. Hart (1984) proposed four types of mantle with different isotopic characteristics, which are depleted MORB mantle (DMM), high-time integrated $^{238}U/^{204}Pb$ or high μ mantle (HIMU), enriched mantle I (EM I), and enriched mantle II (EM II). DMM is the source region of MORB, HIMU may represent ancient metamorphosed oceanic crust, EM I may be the mantle metasomatized by asthenospheric fluids or the mantle formed by the tectonic denudation of Chile Type subducting oceanic crust, and EM II may be the product of mixing by subducting and recycling continental crust and mantle rocks (Hart et al., 1986).

The Tengchong volcanic rocks show significant $^{87}Sr/^{86}$ Sr and $^{143}Nd/^{144}Nd$ negative correlation. In terms of isotope geochemistry, Sr and Nd isotopes used in combination can directly provide much information of rock evolution. No matter if partial melting or fractional crystallization caused the differences in distribution coefficients in Rb and Sr and Nd and Sm, Rb and Nd prefentially entered into melt phase rather than Sr and Sm, respectively (Faure and Mensing, 2005). Therefore, it results in higher Rb/Sr and lower Sm/Nd in the melt, which leads to negative correlation between $^{87}Sr/^{86}Sr$ and $^{143}Nd/^{144}Nd$. Sr-Nd isotopes of the Tengchong samples show that the mantle is an enriched one, which is totally different from MORB, and basalts from NE China and SE China. However, it is difficult to tell how the enriched mantle was

formed just based on the Sr-Nd isotope study. U-Th work reported in Zou et al. (2014) and Hf-Nd work from this study have implication for understanding the nature of this enriched mantle.

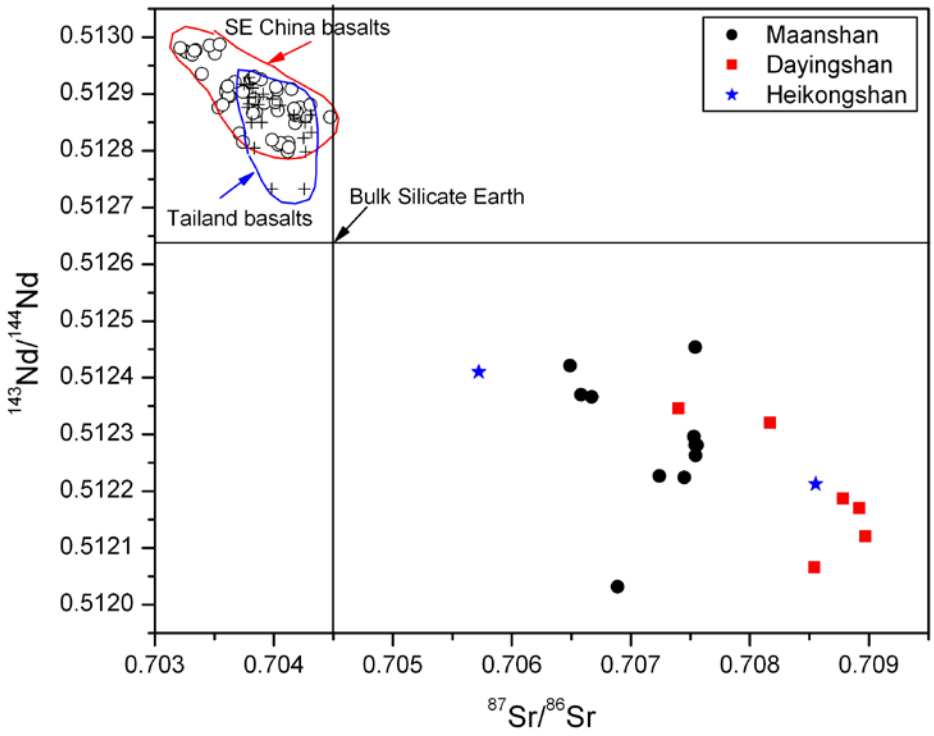

Figure 30. ($^{143}Nd/^{144}Nd$) versus ($^{87}Sr/^{86}Sr$) diagram (Zou et al., 2014). DMM= depleted MORB mantle (Zindler and Hart, 1986); SE China basalts (Tu et al., 1991; Zou and Fan, 2010; Zou et al., 2000); Thailand basalts (Mukasa et al., 1996).

Ultra-high Th/U Magmas

The Tengchong lavas have ultra-high Th/U ratios (9.50 ± 0.69), which is distinct from lavas exposed in other parts of the Tibetan Plateau, such as Ashikule, northwest Tibetan Plateau, northeast China, and Hainan Island (Fig. 31). Since subduction-related fluids are typically enriched in U relative to Th, the ultra-high Th/U ratios are compatible with contributions provided from sediment melts containing high Th/U ratios. High Th/U ratios reflect a mature, weathered source whereas low Th/U ratios indicate immature

continental sediments or organic rich sediments (Plank and Langmuir, 1998). Such ultra-high Th/U sediments must be mature clay-rich sediments or mudstones, because clay-rich mature sediments or mudstones might be the main mature sediments with very high Th/U ratios after extensive weathering to remove U and retain Th (Zou et al., 2014). Neither sandstones nor limestones have high Th/U ratios. Thus, U-Th isotope data provide strong evidence for recycling of mature muds or claystones sediments or mudstone melts, into the mantle source to form the enriched mantle lying beneath Tengchong.

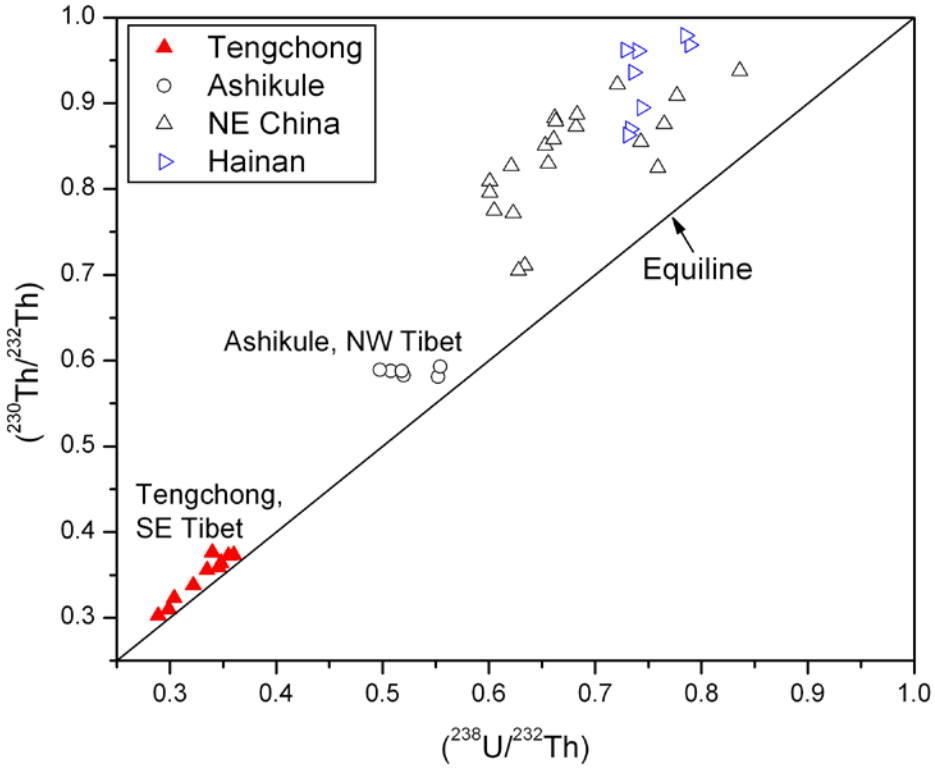

Figure 31. (^{230}Th/^{232}Th) versus (^{238}U/^{232}Th) equiline diagram (Zou et al., 2014). Data sources: Cooper et al. (2002), Zou and Fan (2010), Zou et al. (2008), Zou et al. (2003). Decay constants: Cheng et al. (2000), Jaffey et al. (1971).

Magma Source Sediment Component

The Tengchong volcanic rocks have very distinctive but systematic ε_{Hf} signatures. Taken alone, Hf isotopes cannot distinguish changes due to variations in chemical weathering from those caused by variations in sediment sources. But by combining Lu-Hf with the Sm-Nd isotope system, which exhibit a globally similar behavior but is much less prone to fractionation, it becomes possible to discriminate source-rock components (Bayon et al., 2009). Hence, Hf–Nd isotope analyses of sediments preserved in the geological record provide a powerful tool that can be used to trace the evolution of sediment components through time. The Hf-Nd isotope data for the Tengchong volcanic rocks from this study are reported below in an ε_{Nd} vs. ε_{Hf} diagram, together with other reported data from Zhou et al. (2012) (Fig. 32). Since the Tengchong volcanic rocks have low negative ε_{Nd} values and low negative to positive ε_{Hf} values, they plot above the igneous array, which is also called mantle array, and beneath the seawater array. Thus, lavas from this research and previous study from Zhou et al. (2012) are all plotted close to fine-grained sediments line, which provide strong and sufficient evidence for our hypothesis that the source rocks of Tengchong Holocene volcanic rocks are mantle peridotites metasomatized by melts from fine-grained sediments, such as clay sediments or mudstone, rather than by coarse-grained sediments, like sandstone.

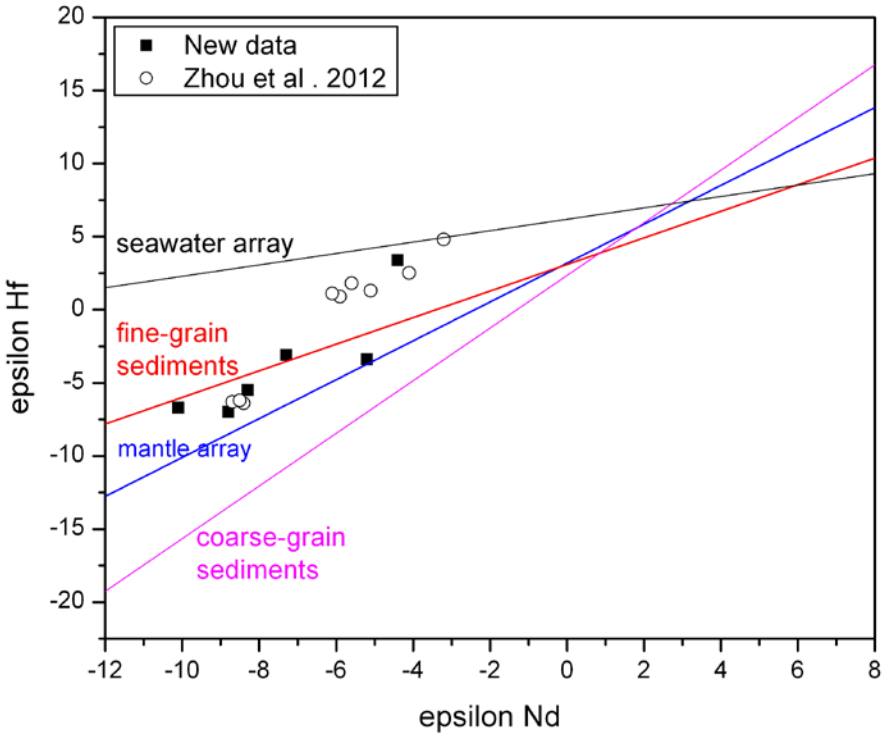

Figure 32. Intial ε_{Nd} and ε_{Hf} values for Tengchong volcanic rocks. Fine-grained sediments (red line) plot along a gentle array. Coarse-grained sediments (pink line) plot along a steep array. The mantle array is the correlation for unwearthered whole-rock data. The seawater array is the correlation for marine Fe-Mn precipitates. Data sources: this paper; previous reseach; Zhou et al., 2012.

CONCLUSIONS

(1) Results of the current study suggest recycling of mature clay sediments or mudstones into the mantle below Tengchong. The implication is that the sediment components in the enriched mantle source for the Tengchong volcanic rocks likely were not coarse-grained sediments, such as sandstones, that should be expected by subduction of a continental margin.

(2) Interpretation of the Hf-Nd isotope systematics is also consistent with the conclusion on mantle source characteristics based on ^{238}U-^{230}Th isotope disequilibrium data of the Tengchong volcanics.

(3) The new constraints on the mantle source rocks from Hf-Nd isotope systematics in Tengchong have implications for the characterization of source rocks for older widespread post-collisional volcanism in other areas of the Tibetan Plateau. Since extrapolation from small to large scales is required to understand global plate tectonics, the author suggests that the utility of these reported results may have application for collisional zones in general.

REFERENCES

Barovich K.M., Beard B.L., Cappel J.B., et al., 1995. A chemical method for hafnium separation from high-Ti whole-rock and zircon samples. Chemical Geology, 121:303-308.

Bayon G., Burton K.W., Soulet G., Vigier N., Dennielou B., Etoubleau J., Ponzevera E., German C.R., Nesbitt R.W., 2009. Hf and Nd isotopes in marine sediments: Constraints on global silicate weathering. Earth and Planetary Science Letters, 277: 318-326.

Bizzarro M, Baker J.A, Ulfbeck D., 2003. A New Digestion and Chemical Separation Technique for Rapid and Highly Reproducible Determination of Lu/Hf and Hf Isotope Ratios in Geological Materials by MC-ICP-MS. Geostand Newslett., 27(2):133-145.

Blichert-Toft J., Albarede F., 1997. The Lu-Hf isotope geochemistry of chondrites and the evolution of the mantle-crust system. Earth and Planet.Sci.Lett., 148: 243-258.

Blichert-Toft J., Chauvel C., Albarede F., 1997. Separation of Hf and Lu for high-precision isotope analysis of rock samples by magnetic sector-multiple collector ICP-MS.Contrib.Mineral,Petrol.,127: 248-260.

Blichert-Toft J., 2001. On the Lu-Hf Isotope Geochemistry of Silicate Rocks. Geostand Newslett., 25(l): 41-56.

Chen F.K., Hegner E., Todt W., 2000. Zircon ages, Nd isotopic and chemical compositions of orthogneisses from the Black Forest, Germany: evidence for a Cambrian magmatic arc. Int Journ Earth Sciences, 88: 791-802.

Chen F.K., Siebel W., Satir M., Terzioglu M.N., Saka K., 2002. Geochronology of the Karadere basement (NW Turkey) and implications for the geological evolution of the Istanbul zone. Int J Earth Sci (Geol Rundsch), 91: 469-481.

Chen F.K., Li Q.L., Wang X.L., Li X.H., 2006. Zircon age and Sr-Nd-Hf isotopic composition of migmatite in the eastern Tengchong block, western Yunnan. Acta Petrologica Sinica, 22 (2): 439-448.

Chen T.F, 2003. The Petrology of the Volcanic Rocks in Tengchong, Yunnan. Sedimentary Geology and Tethyan Geology, 23 (4): 57-61.

Cheng H., Edwards R.L., Hoff J., Gallup C.D., Richards D.A., Asmerom Y., 2000. The half-lives of uranium-234 and thorium-230. Chemical Geology 169, 17-33.

Connelly J.N. et al., 2006. A method for purifying Lu and Hf for analyses by MC-ICP-MS using TODGA resin. Chemical Geology., 233:126-136.

Cooper K.M., Reid M.R., Dunbar N.W., McIntosh W.C., 2002. Origin of mafic magmas beneath northwestern Tibet: constraints from ^{230}Th–^{238}U disequilibria. Geochemistry, Geophysics, Geosystems. http://dx.doi.org/10.1029/2002GC000332.

Corfu F, Noble S.R., 1992. Genesis of Southern Abitibi Green-stone Belt, Superior Province, Canada: Evidence from Zircon-Hf Isotope Analyses using a Single Filament Technique. Geochem Cosmochem Acta., 56: 2081-2097.

Fan Q.C., Sui J.L., Liu R.X., 2001. Sr-Nd Isotopic Geochemistry and Magmatic Evolutions of Wudalianchi Volcano, Tianchi Volcano and Tengchong Volcano. Acta Petrologica et Mineralogica, 20 (3): 233-238.

Faure G, and Mensing T.M, 2005. Isotopes principles and applications. Third Edition. John Wiley & Sons, Inc. p284-294.

Gruau G., Cornichet J., Lecozbouhnik M., 1988. Improved determination of Lu/Hf ratio by chemical-separation of Lu from Yb. Chemical Geology, 72: 353-356.

Halliday A.N., Lee D.C., Christensen J.N., Walder A.J., Freedman P.A., Jones C.E., Hall C.M., Yi W., Teagle D., 1995. Recent developments in inductively coupled plasma magnetic sector multiple collector mass spectrometry. Intl J Mass Spec Ion Proc, 146/147: 21-33.

Halliday A.N., Lee D.C., Christensen J.N., Rehkamper M., Yi W., Luo X.Z., Hall C.M., Ballentine C.J., Pettke T., Stirling C., 1998. Application of multiple collector-ICPMS to cosmochemistry, geochemistry, and paleoceanography. Geochimica Et Cosmochimica Acta, 62 (6): 919-940.

Hart S. R., 1984. A large-scale isotope anomaly in the southern Hemisphere mantle. Nature, 309: 753-757.

Hart S. R., Geriach D. C., White W. M., 1986. A possible new Sr-Nd-Pb mantle array and consequences for mantle mixing. Geochim. Cosmocchim. Act a, 1551-1557.

Jaffey A.H., Flynn K.F., Glendenin L.E., Bentley W.C., Essling A.M., 1971. Precision measurement of half-lives and specific activities of U-235 and U-238. Physical Review C 4, 1889-1906.

Jiang C.S., 1998. Period Division of Volcano Activities in the Cenozoic Era of Tengchong. Journal of Seismological Research, 21 (4): 320-329.

Jiang C.S., Zhou R.Q., Zhou Z.H., Wang Y., 2000. Division of tectonic elements in west Yunnan and its neighboring regions and their features. Journal of Seismological Research 23, 21-29.

Johnson K.T.M, 1998. Experimental determination of parathion coefficients for rare earth and high-field-strength elements between clinopyroxene, garnet, and basaltic melt at high pressures. Contrib.Mineral.Petrol., 133: 60-68.

Kinny P.D, Compston W, Williams I.S, 1991. A reconnaissance ion-probe study of hafnium isotopes in zircons. Geochem Cosmochem Acta 55:849-859.

Kleinhanus I, Kreissig K, Kamber B.S, et al., 2002. Combined Chemical Separation of Lu, Hf, Sm, Nd and REEs from a Single Rock Digest: Precise and Accurate Isotope Determinations of Lu-Hf and Sm-Nd using Multi-collector-ICP-MS. Ana/Chem., 74:67-73.

Knudsen T.L., Griffin W.L., Hartz E.H., et al., 2001. In-situ Hafnium and Lead Isotope Analyses of Detrital Zircons from the Devonian Sedimentary Basin of NE Greenland: a Reeord of Repeated Crustal Reworking.Contrlb.Mineral.Petrol., 141: 83-94.

Le Fevre B, Pin C., 2001. An Extraction Chromatography Method for Hf Separation Prior to Isotopic Analysis using Multiple Collection ICP-Mass Spectrometry. Anal Chem., 73: 2453-2460.

Le Fevre B, Pin C., 2005. A Straightforward Separation Scheme for Concomitant Lu, Hf and Sm, Nd Isotope Ratio and Isotope Dilution Analysis. Analytical Chemica Acta., 543: 209-221.

Li J., 1995. The application of Pearce ratio diagram to the study of Cenozoic volcanics from Tengchong area, Yunnan province. Acta Petrologica Et Mineralogica 14, 203-210.

Li X.H., Qi C.S., Liu Y., Liang X.R., Tu X.L., 2005. Rapid separation of Hf from rock samples for isotope analysis by MC-ICP-MS: A modified single-column extraction chromatography method. Geochimica, 34(2): 109-114.

Liu R.X., 2000. Active Volcanoes of China. Seismological Press, Beijing, pp. 32-44.

Luo W.L., Hu Z.Y., 1983. Petrochemical Characteristic of S-type and I-type Granite in Western Yunnan, China. Yunnan Geology 2(2): 248-259.

Massimo M, Elton L.D., Marcio M.P., Bernhard B., 2010. Combined U-Pb and Lu-Hf isotope analyses by laser ablation MC-ICP-MS: methodology and applications. Annals of the Brazilian Academy of Sciences 82(2): 479-491.

McDonough W.F. and Sun S.S., 1995. The composition of the Earth. Chemical Geology, 120: 223-253.

Mukasa S.B., Fischer G.M., Barr S.M., 1996. The character of the sub-continental mantle in southeast Asia: evidence from isotopic and elemental compositions of extension related Cenozoic basalts in Thailand. In: Basu, A.R., Hart, S.R. (Eds.), Earth Processes: Reading the Isotopic Code. American Geophys. Union, Washington, pp. 233-252.

Munker C.S, Weyer E, Scherer K.M., 2001. Separation of High Field Strength Elements (Nb, Ta, Zr, Hf) and Lu from Rock Samples for MC-ICP-MS Measurements. Geochem Geophys Geosyst., 2:10.1029/2001:GC000183.

Nakamurab N., 1974. Determination of REE, Ba, Fe, Mg, Na and K in carbonaceous and ordinary chondrites. Geochimica et Cosmochimica Acta, 38: 757-775.

Nir-El Y, Lavi N, 1998. Measurement of the half-life of ^{176}Lu. Appl Rad Iso 49: 1653-1655.

Patchett P.J., Tatsumoto M., 1980a. A routine high-precision method for Lu-Hf isotope geochemistry and chronology. Contrib.Mineral.Petrol., 75: 263-268.

Patchett P.J, Tatsumoto M, 1980b. Lu-Hf total-rock isochron for the eucrite meteorites. Nature 288: 571-574.

Patchett P.J, Tatsumoto M., 1980c. A routine high-precision method for Lu-Hf isotope geochemistry and chronology. Contrib Mineral Petrol 75:263-267.

Patchett P.J, Kouvo O, Hedge C.E., Tatsumoto M., 1981. Evolution of continental crust and mantle heterogeneity: evidence from Hf isotopes. Contrib Mineral Petrol 78: 279-297.

Patchett P.J., White W.M., Feldmann H., et al., 1984. Hafnium/rare earth element fractionation in the sedimentary system and crustal recycling into the Earth's Mantle. Earth Planet. Sci. Lett., 69: 365-378.

Plank T., Langmuir C.H., 1998. The chemical composition of subducting sediment and its consequences for the crust and mantle. Chemical Geology 145, 325-394.

Qi X.X., Zhu L.H., Hu Z.C., Li Z.Q., 2011. Zircon SHRIMP U-Pb dating and Lu-Hf isotopic composition for Early Cretaceous plutonic rocks in Tengchong block, southeastern Tibet, and its tectonic implications. Acta Petrologica Sinica，27 (11): 3409-3421.

Salters V.J.M., Hart S.R., 1991. The Mantle Sources of Ocean Ridges, Islands and Arcs: the Hf Isotope Connection. Earth Planet Sci Lett., 104: 364-380.

Salters V.J.M., 1994. $^{176}Hf/^{177}Hf$ determination in small samples by a high-temperature SIMS technique. Anal Chem, 66: 4186-4189.

Scherer E, Münker C, Mezger K, 2001. Calibration of the lutetium-hafnium clock. Science 293: 683-687.

Sguigna A.P, Larabee A.J, Waddington J.C., 1982. The half-life of ^{176}Lu by a γ-γ coincidence measurement. Can J Phys 60: 361-364.

Stevenson R.K., Patchett P.J., 1990. Implications for the Continental Crust from Hf Isotope Systematics of Archean Detrital Zircons.Geochem.Cosmochem.Acta, 54: 1683-1697.

Tapponnier P., Lacassin R., Leloup P.H., Scharer U., Zhong D.L.,Wu H.W., Liu X.H., Ji S.C., Zhang L.S., Zhong J.Y., 1990. The Ailao Shan/Red River metamorphic belt: tertiary left-lateral shear between Indochina and South China. Nature 343: 431-437.

Tu K., Flower M.F.J., Carlson R.W., Zhang M., Xie G., 1991. Sr, Nd, and Pb isotopic compositions of Hainan basalts (south China): implications for a sub-continental lithosphere Dupal source. Geology 19, 567-569.

Tucker S. T., 2011. U-Th dating of zircons from a Holocene volcanic eruption (Dayingshan volcano, Tengchong volcanic field): Insight into magma chamber storage. Auburn University, MS thesis, 88pp.

Tucker S.T., Zou H.B., Fan Q.C., Schmitt A.K., 2013. Ion microprobe dating of zircons from active Dayingshan volcano, Tengchong, SE Tibetan Plateau: Time scales and nature of magma chamber storage. Lithos, 172-173: 214-221.

Ulfbeck D, Baker J.A, Weight T, et al., 2003. Rapid Sample Digestion by Fusion and Chemical Separation of Hf for Isotopic Analysis by MC-ICP-MS. Talanta., 59:365-373.

Vervoort J.D., Blichert-Toft J., 1999. Evolution of the depleted mantle: Hf isotope evidence from juvenile rocks through time.Geochem.Cosmochem.Acta, 63: 533-556.

Vervoort J.D., Patchett P.J., Albarede F., et al., 2000. Hf-Nd isotopic evolution of the lower crust. Earth Planet.Sci.Lett., 181: 115-129.

Vervoort J.D., Patchett P.J., Blichert-Toft J., et al., 1999. Relationships between Lu-Hf and Sm-Nd isotopic systems in the global sedimentary system. Earth Planet. Sci. Lett., 168: 79-99.

Vervoort J.D., Patchett P.J.,Gehrels G.E., et al., 1996. Constraints on early Earth differentiation from hafnium and neodymium isotopes. Nature, 379: 624-627.

Wang H.Z., 1981. China Geotectonic Zone from Mobillism Theory. Earth Science 14(1): 42-46.

Wei H.Q., Sparks R.S.J., Liu R.X., Fan Q.C., Wang Y., Hong H.J., Zhang H., Chen H., Jiang C., Dong J., Zheng Y., Pan Y., 2003. Three active volcanoes in China and their hazards. Journal of Asian Earth Sciences 21, 515-526.

Wilson M., 1989. Igneous Petrogenesis: A Global Tectonic Approach. London (Unwin Hyman), 466pp.

Wu F.Y., Li X.H., Zheng Y.F, Gao S, 2007. Lu-Hf isotopic systematics and their applications in petrology. Acta Petrologica Sinica, 23(2): 185-220.

Xia L.Q., Li X.M., Ma Z.P., Xu X.Y., Xia Z.C., 2011. Cenozoic volcanism and tectonic evolution of the Tibetan Plateau. Gondwana Research, 19: 850-866.

Yang P., 2012. Ion Microprobe Dating of Zircons from Heikongshan Volcano (Tengchong Volcanic Field, Southeast Tibetan Plateau): Time Scale and Nature of Magma Storage. Auburn University, MS thesis, 80pp.

Yang X.J, Pin C., 2000. Determination of Trace Zirconium and Hafnium in Basaltic Rocks by Inductively Coupled Plasma-Atomic Emission Spectrometry after Chemical Separation: An Evaluation of Two Methods Based on Extraction Chromatography. Analyst., 25:453-457.

Yang Y.H., Zhang H.F., Liu Y., Xie L.W., Qi C.S., Tu X.L., 2007. One column procedure for Hf purification in geological samples using anion exchange chromatography and its isotopic analyses by MC-ICP-MS. Acta Petrologica Sinica, 23(2): 227-232.

Yang Y.H., Zhang H.F., Chu Z.Y., Xie L.W., Wu F.Y., 2010. Combined chemical separation of Lu, Hf, Rb, Sr, Sm and Nd from a single rock digest and precise and accurate isotope determinations of Lu-Hf, Rb-Sr and Sm-Nd isotope systems using Multi-Collector ICP-MS and TIMS. International Journal of Mass Spectrometry, 290: 120-126.

Yu H.M., Lin C.Y., Shi L.B., Xu J.D., Chen X.D., 2010. Characteristics and origin of mafic and ultramafic xenoliths in trachyandesite lavas from Heikongshan volcano, Tengchong, Yunnan Province, China. Science in China (Earth Science) 53, 1295-1306.

Zhao Y.W. and Fan Q.C., 2010. Magma origin and evolution of Maanshan volcano, Dayingshan volcano and Heikongshan volcano in Tengchong area. Acta Petrologica Sinica 26 (4), 1133-1140.

Zhao Y.W., Fan Q.C., Li N., Liu G., Zhang L.Y., 2012. Lava Flow Styles in Dayingshan, Maanshan and Heikongshan in Tengchong Volcanic Field. Seismology and Geology, 34 (4): 1-12.

Zhou M.F., Robinson P.T., Wang C.Y., Zhao J.H., Yan D.P., Gao J.F., Malpas J., 2012. Heterogeneous mantle source and magma differentiation of quaternary are-like volcanic rocks from Tengchong, SE margin of the Tibetan Plateau. Contrib Mineral Petrol, 163: 841-860.

Zhou Z.H., Jiang C.S., Li B., 1998. Geochemical features of Sr, Nd and Pb isotopes of volcanic rocks in Cenozoic era in Tengchong, Changbaishan and Wudalianchi, China. Joural of Seismological Research 21, 379-387.

Zhou Z.H., Xiang C.Y., Yang H.L., 2000. Geochemistry of the Isotopes in the Volcanic Rocks in Tengchong, China. Journal of Seismological Research, 23 (2): 194-200.

Zhu B.Q., Mao C.X., Lugmair G.W., Macdougall J.D., 1983. Isotopic and geochemical evidence for the origin of Plio-Pleistocene volcanic rocks near the Indo-Eurasian collisional margin at Tengchong, China. Earth and Planetary Science Letters, 65: 263-275.

Zhu D.C., Pan G.T., Mo X.X., Duan L.P., Liao Z.L., Wang L.Q., 2003. Sr-Nd-Pb isotopic vatiations of the Cenozoic volcanic rocks from the Qinghai-Xizang Plateau and its adjacent areas. Sedimentary Geology and Tethyan Geology 23, 1-11.

Zindler A. and Hart S.R., 1986. Chemical geodynamics. Annual Review of Earth and Planetary Sciences 14, 493-571.

Zou H.B., Zindler A., Xu X.S., Qi Q., 2000. Major, trace element, and Nd, Sr and Pb isotope studies of Cenozoic basalts in SE China: mantle source, regional variations, and tectonic siginificance. Chemical Geology 171, 33-47.

Zou H.B., Reid M.R., Liu Y.S., Yao Y.P., Xu X.S., Fan Q.C., 2003. Constraints on the origin of historic potassic basalts from northeast China by U-Th disequilibrium data. Chemical Geology 200, 189-201.

Zou H.B., Fan Q.C., Yao Y.P., 2008. U-Th systematics of dispersed young volcanoes in NE China: asthenosphere upwelling caused by piling up and upward thickening of stagnant Pacific slab. Chemical Geology 255, 134-142.

Zou H.B., Fan Q.C., 2010. U-Th isotopes in Hainan basalts: implications for sub-asthenospheric origin of EM2 mantle endmember and the dynamics of melting beneath Hainan Island. Lithos 116, 145-152.

Zou H.B., Fan Q.C., Schmitt A.K., Sui J.L., 2010. U-Th dating of zircons from Holocene potassic andesites (Maanshan volcano, Tengchong, SE Tibetan Plateau) by depth profiling: Time scale and nature of magma storage. Lithos 118, 202-210.

Zou H.B. and Fan Q.C., 2011. Uranium-thorium isotope disequilibrium in young volcanic rocks from China. Acta Petrologica Sinica 27, 2821-2826.

Zou H.B., Shen C.C., Fan Q.C., Lin K., 2014. U-series disequilibrium in young Tengchong volcanics: Recycling of mature clay sediments or mudstones into the SE Tibetan mantle. Lithos, 192-195: 132-141.

APPENDIX

Table 7. Major and trace element data of Tengchong volcanic rocks from Chen et al., 2006.

Sample	03BS12	03BS13	03BS14	03BS15	03BS16	03BS17
SiO_2	72.95	65.75	68.78	65.64	63.95	65.73
TiO_2	0.39	0.52	0.52	0.63	0.71	0.74
Al_2O_3	13.33	17.39	14.36	14.85	16.05	15.73
Fe_2O_3	2.29	3.46	3.79	4.79	4.52	4.99
MnO	0.05	0.05	0.07	0.08	0.09	0.11
MgO	0.45	0.87	1.57	2.35	1.05	1.08
CaO	1.27	3.27	3.28	4.19	2.76	2.49
Na_2O	2.75	3.63	2.67	2.76	4.14	4.36
K_2O	4.72	3.23	3.34	3.28	3.76	3.14
P_2O_5	0.11	0.11	0.13	0.16	0.21	0.22
LOI	1.02	1.27	0.93	0.70	2.63	0.70
Total	99.33	99.55	99.44	99.43	99.86	99.46
Ba	318	632		413		
Cs	14.8	16.8		15.4		
Nb	48.2	17.6		14.9		
Ni	4.99	11.4		15.6		
Rb	457	127		191		
Sr	76.2	370		274		
Y	34.8	15.3		21.0		
Zr	306	368		189		
Hf	10.1	10.1		5.75		
Pb	60.1	31.3		18.0		
Th	77.5	20.0		22.4		
U	10.4	5.34		3.92		
La	108	25.8		48.4		
Ce	212	54.4		89.6		
Pr	23.7	5.46		9.02		
Nd	80.1	18.8		30.8		
Sm	13.6	3.81		5.31		
Eu	0.82	0.94		1.14		
Gd	10.5	3.16		4.54		
Tb	1.48	0.49		0.66		
Dy	7.67	3.14		3.94		
Ho	1.36	0.65		0.82		
Er	3.68	2.11		2.38		
Tm	0.50	0.32		0.34		
Yb	3.02	2.43		2.21		
Lu	0.45	0.39		0.34		

Table 8. Major element data of Tengchong volcanic rocks from Yu et al., 2010.

Sample	**09H3**	**09H2**	**09H23**	**09H11**	**09H1**	**09H4**	**09H6**	**09H13**	**09H5**	**09H9**	**09H12**	**09H10**
SiO_2	50.5	54.6	57.4	60.0	58.2	58.8	57.9	57.7	59.0	58.1	65.9	66.3
Al_2O_3	18.7	17.4	16.9	15.9	16.5	16.4	16.5	16.5	16.4	16.6	15.1	14.9
TiO_2	1.54	1.17	1.10	1.05	0.94	1.08	1.15	1.07	0.87	1.09	0.61	0.66
Fe_2O_3	2.09	1.64	2.25	1.22	1.45	1.05	0.97	0.84	1.55	1.16	0.85	0.78
FeO	6.75	6.01	3.90	4.20	4.77	4.98	5.03	5.01	4.14	4.89	2.95	2.92
CaO	6.33	6.96	5.92	5.18	5.40	5.70	5.81	5.66	5.51	5.62	3.20	3.17
MgO	4.91	4.63	3.77	3.57	4.15	3.93	3.92	3.96	3.93	3.99	1.85	1.81
K_2O	2.05	2.59	3.17	3.74	3.31	3.42	3.38	3.42	3.42	3.35	4.54	4.40
Na_2O	3.44	3.49	3.31	3.66	3.35	3.52	3.49	3.59	3.42	3.42	3.59	3.42
MnO	0.14	0.13	0.11	0.11	0.11	0.11	0.11	0.11	0.10	0.11	0.08	0.08
P_2O_5	0.42	0.30	0.42	0.41	0.43	0.44	0.42	0.43	0.38	0.42	0.23	0.22
H_2O^+	2.60	0.69	0.82	0.40	0.75	0.26	0.23	0.68	0.58	0.30	0.16	0.48
LOI	2.97	1.03	1.14	0.65	1.08	0.41	0.77	1.01	0.98	0.76	0.52	0.70
Total	99.8	100.0	99.4	99.7	99.6	99.8	99.4	99.3	99.8	99.5	99.4	99.3

Table 9. Major and trace element data of Tengchong volcanic rocks from Zhao et al., 2010.

Sample	08YTC01	08YTC04	08YTC11	08YTC13	08YTC14	08YTC15	08YTC17
SiO_2	58.79	58.56	58.77	58.37	64.06	61.98	63.65
TiO_2	1.36	1.4	1.33	1.41	1.00	1.18	1.04
Al_2O_3	16.76	16.93	16.75	17.13	15.86	16.36	16.07
Fe_2O_3	1.69	1.83	1.38	2.56	1.39	1.47	1.54
FeO	4.81	4.67	4.96	3.79	3.48	4.07	3.51
MnO	0.11	0.11	0.11	0.10	0.09	0.09	0.09
MgO	3.76	3.74	4.24	3.58	2.17	2.66	2.27
CaO	5.63	5.94	5.98	5.95	3.90	4.77	4.11
Na_2O	3.58	3.46	3.30	3.52	3.51	3.48	3.35
K_2O	3.00	2.89	2.76	3.15	3.69	3.55	3.73
P_2O_5	0.47	0.47	0.45	0.48	0.33	0.40	0.35
Total	99.96	100.0	100.0	100.0	99.48	100.0	99.71
La	65.9		73.7			78.4	
Ce	125		145			154	
Pr	14.3		16.6			17.2	
Nd	49.5		56.8			59.5	
Sm	8.73		9.73			10.0	
Eu	1.79		1.93			1.78	
Gd	7.05		7.06			7.40	
Tb	0.98		1.02			1.05	
Dy	5.62		5.53			5.82	
Ho	1.11		1.07			1.12	
Er	2.88		2.80			3.01	
Tm	0.43		0.39			0.43	
Yb	2.73		2.42			2.60	
Lu	0.42		0.38			0.41	
Ba	780		928			897	
Rb	105		99			127	
Sr	534		523			433	
Y	27.1		26.1			27.2	
Zr	313		311			320	
Nb	27.0		28.0			27.3	
Th	23.9		23.3			32.7	
Pb	20.1		22.6			26.1	
Ga	20.2		21.4			20.9	
Zn	71.4		83.8			72.7	
Cu	18.7		22.2			17.0	
Ni	35.6		59.8			24.2	
V	106		116			92	
Cr	91		140			97	
Hf	8.64		8.89			9.40	
Cs	1.94		1.32			2.06	
Sc	15.5		16.3			12.7	
Ta	1.67		1.66			1.72	
Co	17.5		20.4			13.8	
Li	16.9		16.2			21.3	
Be	2.18		2.05			2.43	

Table 10. Major and trace element data of Tengchong volcanic rocks from Zhou et al., 2012.

Sample	TC-27	TC-30	TC-31	TC-32	TC-35	TC-36	TC-39	TC-41	TC-43	TC-57	TC-2	TC-5	TC-7	TC-8	TC-9	TC-11	TC-12	TC-15	TC-16	TC-19	TC-21	TC-22	TC-23	TC-26
SiO_2	51.68	52.47	55.53	51.88	49.29	49.87	52.61	50.01	50.16	54.55	52.47	53.04	53.34	54.59	55.80	55.02	58.75	57.13	56.89	60.47	58.35	58.69	57.33	57.34
TiO_2	1.42	1.44	1.13	1.39	1.64	1.42	1.28	1.43	1.43	1.13	1.34	1.31	1.33	1.23	1.16	1.19	1.01	1.12	1.13	0.93	1.07	1.07	1.10	1.10
Al_2O_3	16.57	16.65	16.19	16.52	17.37	17.13	16.94	17.26	17.31	16.50	17.54	17.16	17.78	16.66	16.35	16.43	16.21	16.36	16.34	15.78	16.25	16.48	16.38	16.59
Fe_2O_3	9.54	9.86	7.83	9.67	10.77	9.06	7.49	9.00	9.01	7.97	8.49	8.31	8.40	7.83	7.40	7.54	5.94	6.52	6.56	5.52	6.28	6.24	6.44	6.42
MnO	0.15	0.14	0.12	0.16	0.16	0.15	0.13	0.17	0.15	0.13	0.14	0.14	0.14	0.13	0.12	0.13	0.11	0.11	0.11	0.10	0.11	0.11	0.11	0.11
MgO	5.35	5.56	4.52	5.35	6.19	5.63	5.81	5.70	5.48	4.84	5.41	5.33	5.32	4.88	4.43	4.67	3.48	3.79	3.78	3.02	3.70	3.55	3.76	3.86
CaO	7.10	7.39	6.20	6.76	8.88	8.81	6.67	8.89	9.09	6.66	7.52	7.50	7.28	7.10	6.62	6.71	5.31	5.86	5.94	4.85	5.66	5.60	5.81	5.83
Na_2O	3.90	3.81	3.79	3.74	3.39	3.85	3.86	3.34	3.49	3.47	3.61	3.98	3.57	4.11	3.53	4.32	4.24	3.58	3.93	3.73	3.80	3.54	3.95	3.85
K_2O	2.30	2.26	2.97	2.34	1.46	2.05	3.31	1.94	1.99	2.79	2.27	2.46	2.34	2.68	2.96	3.00	3.51	3.25	3.26	3.79	3.42	3.45	3.35	3.33
P_2O_5	0.40	0.39	0.25	0.40	0.41	0.45	0.57	0.48	0.47	0.26	0.38	0.37	0.37	0.34	0.32	0.34	0.39	0.45	0.45	0.36	0.43	0.43	0.45	0.45
LOI	0.53	0.00	0.54	0.83	-0.03	0.41	0.49	0.97	0.82	0.69	0.70	0.32	-0.06	0.36	0.50	0.47	0.53	0.61	0.67	0.60	0.42	0.28	0.28	0.37
Total	98.95	99.90	99.06	99.03	99.54	98.82	99.15	99.20	99.39	98.99	99.88	99.92	99.81	99.90	99.20	99.83	99.47	98.78	99.05	99.16	99.49	99.46	98.97	99.25
Sc	19.5	20.1	18.1	21.0	22.0	22.6	17.10	22.8	23.4	19.6	20.2	20.3	21.0	20.8	18.9	20.4	15.4	14.9	16.4	14.5	16.8	16.8	15.6	15.5
V	112	119	103	114	174	159	131.0	159	168	115	142	132	148	142	128	134	101	103	106	89	111	108	109	100
Cr	119	122	117	128	38	127	99	138	139	130	131	131	135	129	116	119	55	60	60	53	73	63	59	60
Co	27.0	28.0	24.3	28.2	37.8	28.2	24	29.5	30.1	26.4	28.1	28.5	29.2	27.7	25.3	26.7	17.6	18.2	18.4	15.7	19.5	19.2	20.3	18.0
Ni	40.7	51.1	39.5	42.9	45.5	55.4	78.5	60.3	58.8	44.2	59.2	59.3	61.4	60.2	53.7	54.7	52.5	57.1	54.6	46.5	62.8	93.2	59.0	57.2
Cu	20.6	22.5	23.9	22.3	34.5	37.1	19.0	33.0	35.3	25.2	23.9	29.1	25.9	30.7	27.9	31.0	22.4	22.9	19.9	18.3	25.2	24.6	24.7	21.6
Zn	121	124	99	134	120	108	87.0	121	112	122	99	102	103	110	93	97	97	101	97	115	123	124	153	115
Rb	48.2	44.5	85.7	46.1	20.2	36.8	81	33.3	37.3	78.4	37.7	49.5	47.3	78.4	94.8	86.3	119.1	96.4	96.1	138.4	111.6	111.9	98.8	96.50
Sr	397	412	360	396	560	649	758	689	683	397	497	497	473	476	452	459	523	550	554	467	553	555	551	550
Y	26.7	26.2	25.5	28.1	24.1	23.9	23.3	24.2	24.5	27.2	24.9	24.8	26.1	25.5	25.4	25.4	26.7	25.9	26.3	26.4	27.6	27.0	26.3	25.5
Zr	187	184	233	202	142	173	198	174	178	241	204	202	215	210	206	209	326	331	334	304	336	339	330	324
Nb	24.1	23.6	23.4	26.2	18.4	23.2	32.4	23.5	23.4	24.0	23.5	23.5	24.3	23.7	24.1	24.0	29.3	29.1	29.4	29.5	30.4	30.8	29.6	28.7
Ba	440	437	514	470	406	765	1061	833	773	527	516	507	504	478	484	482	932	1012	1005	844	933	914	968	992
La	31.5	32.0	47.4	34.5	26.8	41.8	66.7	41.9	41.6	48.0	39.1	38.4	39.3	39.3	43.4	41.9	72.9	73.6	73.0	71.0	69.5	70.8	70.5	73.7
Ce	62.0	61.3	91.0	64.8	51.3	78.0	126.3	80.6	78.5	88.3	75.4	73.4	77.3	76.0	83.5	81.2	140.5	143.5	144.3	138.9	136.5	138.4	139.8	140.7
Pr	7.3	7.2	9.6	7.8	6.0	8.8	13.2	8.9	9.0	9.8	8.4	8.2	8.5	8.2	9.0	8.8	14.7	15.1	15.1	14.5	14.1	14.2	14.5	14.9
Nd	28.9	28.2	34.5	30.1	24.0	33.5	48.0	33.9	33.7	35.2	31.7	30.6	31.2	30.2	32.5	31.5	53.1	54.8	55.1	51.0	50.9	50.3	52.8	54.1
Sm	5.99	6.10	6.36	6.40	5.21	6.19	7.80	6.43	6.25	6.61	6.06	5.92	5.90	5.75	6.01	6.11	9.04	9.39	9.20	8.39	8.73	8.41	8.79	9.18
Eu	1.71	1.69	1.39	1.67	1.62	1.79	1.91	1.80	1.73	1.46	1.61	1.49	1.44	1.42	1.31	1.39	1.78	1.97	1.90	1.57	1.81	1.73	1.82	1.85
Gd	5.92	5.89	5.54	6.00	5.25	5.69	5.75	5.50	5.44	5.76	5.46	5.33	5.16	4.92	4.93	5.21	6.76	7.05	6.91	6.31	6.47	6.29	6.80	6.76
Tb	0.95	0.94	0.87	0.95	0.81	0.86	0.91	0.85	0.84	0.88	0.86	0.82	0.84	0.80	0.79	0.81	0.97	1.01	1.03	0.93	0.95	0.95	0.97	1.02
Dy	5.45	5.37	4.86	5.39	4.57	4.78	4.75	4.80	4.79	4.91	4.93	4.69	4.66	4.42	4.34	4.36	5.12	5.22	5.23	4.87	4.72	4.69	5.00	5.21
Ho	1.05	1.03	0.94	1.03	0.89	0.92	0.91	0.93	0.92	0.98	0.93	0.91	0.90	0.84	0.83	0.85	0.95	0.95	0.95	0.89	0.90	0.86	0.91	0.98
Er	3.02	2.99	2.83	3.05	2.64	2.77	2.73	2.78	2.77	2.84	2.80	2.73	2.59	2.46	2.45	2.55	2.81	2.87	2.87	2.68	2.56	2.49	2.68	2.86
Tm	0.41	0.40	0.39	0.41	0.35	0.36	0.36	0.37	0.38	0.40	0.38	0.37	0.36	0.34	0.34	0.33	0.37	0.37	0.38	0.35	0.34	0.34	0.36	0.38
Yb	2.62	2.59	2.54	2.77	2.34	2.43	2.44	2.52	2.43	2.59	2.47	2.44	2.19	2.19	2.20	2.25	2.46	2.52	2.50	2.27	2.17	2.10	2.36	2.46
Lu	0.38	0.38	0.37	0.40	0.33	0.36	0.36	0.36	0.35	0.36	0.37	0.34	0.34	0.31	0.32	0.33	0.36	0.35	0.35	0.34	0.31	0.32	0.33	0.37
Hf	4.62	4.53	5.51	4.82	3.46	4.20	5.07	4.10	3.95	5.54	4.70	4.63	4.49	4.23	4.42	4.51	7.40	8.09	8.00	6.54	6.86	6.67	7.56	7.86
Ta	1.39	1.36	1.39	1.34	0.95	1.26	1.89	1.31	1.23	1.31	1.37	1.32	1.27	1.21	1.21	1.25	1.67	1.65	1.63	1.74	1.47	1.44	1.49	1.67
Pb	8.82	8.97	15.32	8.78	3.94	8.61	17.0	34.6	8.3	14.5	12.0	11.4	10.9	11.0	12.2	11.9	23.0	21.2	21.8	22.2	17.8	17.3	19.7	22.6
Th	11.4	11.8	25.7	11.0	4.6	9.4	22.7	9.4	8.3	19.4	16.3	14.5	13.1	12.4	14.4	14.2	25.5	24.2	23.1	22.8	16.5	16.4	19.3	25.6
U	1.99	3.05	5.53	1.74	1.89	2.18	1.87	1.50	1.47	1.87	1.87	1.67	1.77	1.78	1.96	1.96	3.24	2.83	2.87	3.15	2.57	2.54	3.11	3.53